JGR Atmospheres

RESEARCH ARTICLE
10.1029/2024JD042828

A European Hail and Lightning Climatology From an 11-Year Kilometer-Scale Regional Climate Simulation

R. Cui[1,2], I. Thurnherr[1], P. Velasquez[1], K. P. Brennan[1], M. Leclair[1], A. Mazzoleni[3], T. Schmid[3,4], H. Wernli[1], and C. Schär[1]

[1]Institute for Atmospheric and Climate Science, ETH Zurich, Zurich, Switzerland, [2]Agroscope, Climate and Agriculture, Zurich, Switzerland, [3]Institute for Environmental Decisions, ETH Zurich, Zurich, Switzerland, [4]Federal Office of Meteorology and Climatology MeteoSwiss, Zurich, Switzerland

Abstract Hail and lightning, associated with severe convective storms, can cause extensive damage to infrastructure, agriculture, and ecosystems. Because of the small scale of these storms and the complexity of the involved processes, observing and modeling convective storms is challenging. The potential of online diagnostics in convection-permitting models to simulate hail and lightning, especially over climatic time scales and extended regions, has not yet been fully exploited. To address this gap, we present a European-wide hail and lightning climatology (2011–2021) using the Consortium for Small Scale Modeling (COSMO) regional climate model with a horizontal grid spacing of 2.2 km, coupled with a hail growth model (HAILCAST) and the lightning potential index (LPI) diagnostics. We further developed a new European-wide hail product based on the Operational Program for the Exchange of Weather Radar Information (OPERA) composite. Model validation against observations demonstrates an overall good performance in simulating hail and lightning on spatial, seasonal, and diurnal scales. The highest hail frequencies occur during summer along the slopes of high mountain ridges, such as the Alps, Pyrenees, and the Carpathians, aligning with observed lightning hotspots in Europe. In autumn, hail and lightning occur predominantly over the Mediterranean and along the Adriatic coast. Severe hail events with a maximum hail diameter larger than 20 mm mainly occur in the Po Valley, western Spain, and Eastern Europe. This 11-year simulation provides a European-wide data set of severe convective storms and their properties, serving as a basis for further studies of convective events and their impacts.

Plain Language Summary Severe convective storms often cause hail and lightning, which can lead to significant damage. Such events are difficult to observe and model due to their small scale and complexity. To address this, we performed an 11-year long high-resolution climate simulations (2.2 km) using COSMO with hail and lightning diagnostics. Additionally, we developed a European-wide hail data set based on the Operational Program for the Exchange of Weather Radar Information radar composite. The model was validated against radar- and crowd-sourced data, demonstrating good performance. Hail and lightning are most frequent along mountain ranges such as the Alps and Pyrenees in summer, and in autumn, storms shift to the Mediterranean. This 11-year data set offers valuable insights into the characteristics of severe storms across Europe, supporting further research on factors driving these events and their impact in the context of climate change.

R. Cui and I. Thurnherr contributed equally to this work.

Key Points:

- We present a European-wide climatology of hail and lightning based on a convection-permitting climate simulation
- We introduce a new radar-based European-wide hail data set for the years 2013–2021

Supporting Information:

Supporting Information may be found in the online version of this article.

Correspondence to:

R. Cui,
ruoyi.cui@agroscope.admin.ch

Citation:

Cui, R., Thurnherr, I., Velasquez, P., Brennan, K. P., Leclair, M., Mazzoleni, A., et al. (2025). A European hail and lightning climatology from an 11-year kilometer-scale regional climate simulation. *Journal of Geophysical Research: Atmospheres*, *130*, e2024JD042828. https://doi.org/10.1029/2024JD042828

Received 1 NOV 2024
Accepted 30 MAY 2025

Author Contributions:

Conceptualization: H. Wernli, C. Schär
Data curation: R. Cui, I. Thurnherr, P. Velasquez, K. P. Brennan, A. Mazzoleni, T. Schmid
Funding acquisition: H. Wernli, C. Schär
Investigation: R. Cui, I. Thurnherr
Methodology: R. Cui, I. Thurnherr, P. Velasquez, K. P. Brennan
Software: M. Leclair
Supervision: H. Wernli, C. Schär
Visualization: R. Cui, K. P. Brennan
Writing – original draft: I. Thurnherr
Writing – review & editing: R. Cui, I. Thurnherr, P. Velasquez, K. P. Brennan, M. Leclair, A. Mazzoleni, T. Schmid, H. Wernli, C. Schär

1. Introduction

Severe convective storms, along with associated hazards such as hail and lightning, can have significant economic and societal impacts, causing damage to infrastructure, agriculture, and ecosystems (e.g., Carver et al., 2017; Dessens, 1986; Portmann et al., 2024; Schmid et al., 2024). Reanalysis data indicate a positive trend in the occurrence frequency of environmental conditions favoring convective storms across central to eastern Europe in the last decades (Taszarek et al., 2021). Moreover, the probability of convective storm-related hazards such as hail and lightning is likely to increase with climate change (Rädler et al., 2019). Understanding the distribution and drivers of these events, as well as accurately representing them in climate models, is therefore crucial.

The observation and modeling of convective storms are challenging due to their small scale and the complex processes involved. To overcome these challenges, studies often rely on proxies to assess storm-prone environments (e.g., Taszarek et al., 2019). Even more difficult than studying convective storm environments is the task of observing and modeling storm-related hazards such as hail and lightning. Convective events with hail and lightning are rare and have limited spatial extent, making direct observations difficult. However, lightning can be observed through the measurement of lightning-induced radio frequency electromagnetic fields, which can

pinpoint lightning occurrences from thousands of kilometers away with a horizontal resolution of a few kilometers or less (Bennett et al., 2011). Lightning location systems, such as the Arrival Time Differencing network (ATDnet), provide continuous, European-wide observations using a network of very low frequency sferics sensors (Anderson & Klugmann, 2014). The extensive spatial coverage of these lightning observations enables the tracking of convective systems and serves as a valuable filtering criterion for identifying convective environments (Fluck et al., 2021).

Direct hail observations primarily rely on crowd-sourced reports (e.g., Wells et al., 2024), as well as hail pad and sensor measurements. However, crowd-sourced reports are skewed by population density and varying reporting frequencies over time (Barras et al., 2019; Cifelli et al., 2005; Dotzek et al., 2009; Groenemeijer et al., 2017). Hail pad and sensor observations, while valuable, are sparse and only represent small areas (Blašković et al., 2023; Jelić et al., 2020; Löffler-Mang et al., 2011; Manzato, Cicogna, et al., 2022; Nisi et al., 2016). To address these limitations, radar- and satellite-based remote sensing technologies are employed to continuously monitor hail probability and occurrence. Radar-based hail estimates rely on the vertical distance of high radar reflectivity signals and the melting level height (e.g., Kunz & Kugel, 2015; Nisi et al., 2016; Waldvogel et al., 1979). The radar reflectivity products needed for such hail estimates are often only available for specific regions provided by national meteorological services. Satellite-based data sets detect hail via overshooting cloud tops, although the accuracy of these data sets is often compromised by the challenges of translating cloud top height into hail occurrence frequency (Cecil, 2009). Moreover, these data sets typically offer only coarse resolutions. As a result, hail climatologies based on observations across Europe are either biased due to hail sampling issues (Groenemeijer et al., 2017; Punge & Kunz, 2016) or are limited to specific countries or regions (e.g., Barras et al., 2019; Fluck et al., 2021; Giaiotti et al., 2003).

The Operational Program for the Exchange of Weather Radar Information (OPERA) provides a European-wide radar composite by combining radar products from national meteorological and hydrological services throughout Europe (Huuskonen et al., 2014). However, the OPERA data set has not yet been used to produce a comprehensive hail product due to the lack of volumetric (3D) radar reflectivity information and the challenges of processing heterogeneous radar networks with different technologies across regions. Consequently, despite the clear need for a European-wide, continuous hail observation data set to better characterize hail risk and validate hail proxies and simulations, no such product is currently available.

To fill the spatial and temporal gaps in hail observations, model-based hail climatologies have been developed to provide European-wide hail distributions. These climatologies are derived using various offline methods, including empirical hail models (Hand & Cappelluti, 2011; Sanderson et al., 2015), stochastic or logistic models (Mohr et al., 2015; Punge et al., 2014), and hail proxies based on environmental variables (Kahraman et al., 2024; Prein & Holland, 2018). Except for the work by Kahraman et al. (2024), previous studies relied on reanalyzes or climate model simulations with parameterized convection. However, these models often struggle to accurately represent the strength and diurnal cycle of convective systems—a limitation that can be overcome by explicitly resolving convection in high-resolution climate model simulations (Leutwyler et al., 2017; Prein et al., 2015). Over the past decade, kilometer-scale regional climate simulations have become increasingly available (Coppola et al., 2018; Leutwyler et al., 2017; Prein et al., 2015). These high-resolution simulations with regional convection-permitting models (CPMs) explicitly resolve convection and have a better representation of orography, leading to a more accurate representation of convective precipitation processes and associated phenomena. In particular, using km-scale simulations enabled for the first time an adequate simulation of short-term heavy precipitation events with durations of 10 min to 3 hr (Ban et al., 2014; Estermann et al., 2025; Fowler et al., 2021; Kendon et al., 2014; Vergara-Temprado et al., 2021). In addition, studies found better performance in representing surface winds and cloud cover (Belušić et al., 2018; Hentgen et al., 2019).

Hail and lightning diagnostics can be simulated online in numerical models, which is particularly effective with CPM simulations that accurately represent convective storms. Online diagnostics utilize the full range of prognostic fields at each model time step (usually less than 1 min) in contrast to offline diagnostics, which can only access a limited set of output fields, typically available at hourly or coarser temporal resolutions. For the simulation of hail, several approaches have been developed and applied, including a coupled 1D model that uses vertical atmospheric profiles to simulate hailstone growth within updrafts and melting below the cloud base (Brimelow et al., 2002; Jewell & Brimelow, 2009). Other approaches use either a combined graupel/hail hydrometeor category in a one-moment bulk microphysics scheme (Trapp et al., 2019), or explicitly represent hail

using a two-moment bulk microphysics scheme (e.g., Labriola et al., 2019; Milbrandt & Yau, 2006; Noppel et al., 2010; Toker et al., 2021; Yin et al., 2021). As high spatial resolution is required to accurately simulate convective systems, hail simulations are computationally expensive. Although simulations using a two-moment bulk microphysics scheme are particularly resource-intensive (Mansell et al., 2010), vertical column models such as HAILCAST (Jewell & Brimelow, 2009) and the quasi-Lagrangian "convection-allowing model"—(CAM-) HAILCAST (Adams-Selin & Ziegler, 2016; Adams-Selin et al., 2019) are less computationally demanding. CAM-HAILCAST has shown good performance in case studies when integrated in high-resolution CPMs, such as the advanced research version of the Weather Research and Forecasting (WRF) model (Adams-Selin & Ziegler, 2016; Trefalt et al., 2018) or the Consortium for Small Scale Modeling (COSMO) model (Brennan et al., 2024; Cui et al., 2023; Malečić et al., 2023). These promising results from simulating hail with CAM-HAILCAST in case studies indicate the potential for its use in longer, climatological CPM simulations, enabling more comprehensive climatological analyses.

Simulating lightning in numerical models often relies on atmospheric stability and thermodynamics indices, such as the K-index (Sturtevant, 1995), lifted index (Galway, 1956), and the cloud physics thunder parameter (Bright et al., 2005). More sophisticated approaches to modeling lightning have emerged, benefiting from the high-resolution models. For instance, McCaul et al. (2009) linked lightning flash rate to graupel flux and the integration of solid hydrometers within the column. Furthermore, the lightning potential index (LPI, Yair et al., 2010; Brisson et al., 2021) considers the ratio of modeled solid and supercooled liquid hydrometeors within the charging zone, along with the vertical velocity, to estimate lightning activity. These lightning diagnostics, when implemented in CPMs, have demonstrated a good representation of lightning activity across Europe (Cui et al., 2023; Kahraman et al., 2022; Yair et al., 2010).

The potential of CAM-HAILCAST and LPI to simulate hail and lightning in CPMs has not yet been exploited on climatological time scales and over extended regions. To address this gap, we present an 11-year climatology of hail and lightning based on a European-wide CPM simulation, utilizing CAM-HAILCAST and LPI integrated into the COSMO model. We validate and compare these model-based climatologies against a new European-wide data set of hail derived from OPERA radar composite and lightning observations from ATDnet.

Section 2 provides an overview of the COSMO model and diagnostics, and the observational data sets (temperature, precipitation, hail, and lightning) used for the model validation. Section 3 evaluates the simulated seasonal climatologies of temperature and precipitation. Sections 4 and 5 present the model-based European climatologies of hail and lightning, respectively. Conclusions and a brief outlook are given in Section 6.

2. Data and Methods

2.1. Model Description and Configuration

The simulation is performed with the non-hydrostatic COSMO model (http://www.cosmo-model.org). Specifically, we use COSMO v6, a climate version of COSMO (Baldauf et al., 2011) with CAM-HAILCAST and LPI diagnostics. COSMO v6 is optimized for hybrid CPU-GPU architectures (Leutwyler et al., 2017; Schär et al., 2020). To this end, the dynamical core was rewritten in the domain-specific language GridTools (Afanasyev et al., 2021), and the parameterizations were ported via compiler directives (Lapillonne & Fuhrer, 2014). The COSMO model has been used for more than 10 years by the Federal Office of Meteorology and Climatology Meteoswiss (MeteoSwiss) as their numerical weather prediction model, until it was superseded by the Icosahedral Nonhydrostatic Weather and Climate Model (ICON, Zängl et al., 2015) in June 2024. Hereafter, COSMO v6 is referred to as COSMO for simplicity.

The model configuration follows a two-step nesting approach, with a horizontal grid spacing of 12 km in the outer domain and subsequently of 2.2 km in the inner domain (Figure 1). Boundary conditions for the 12 km simulation are provided by 3-hourly ERA5 reanalyzes (Hersbach et al., 2020). Both simulations feature 60 terrain-following hybrid vertical levels. Cloud microphysics is parametrized using the one-moment bulk scheme after Reinhardt and Seifert (2006), with prognostic cloud water, cloud ice, graupel, rain, and snow. In the outer-domain 12 km simulation, shallow and deep convection are parameterized using the Tiedtke (1989) convection scheme. For the inner-domain 2.2 km simulation, the convection parameterization schemes are switched off to treat convection explicitly. This COSMO model setup, with km-scale grid spacing, has been tested and applied in many climate

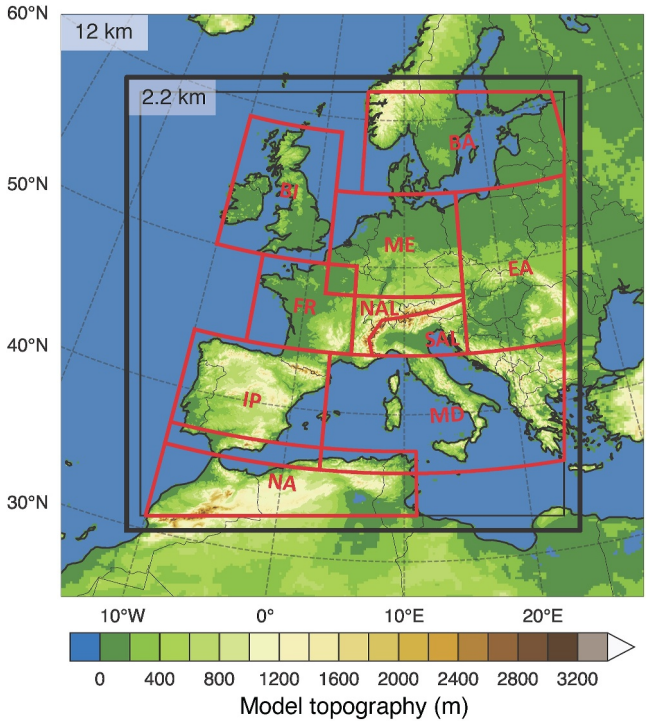

Figure 1. Model topography and domains, with ocean/sea indicated in blue. The full outer domain with 12 km grid spacing is shown, with the bold black box indicating the inner domain with 2.2 km grid spacing. The analysis domain (thin black box) and nine subdomains (red boxes) are also depicted: British Isles [BI], Baltic region [BA], France [FR], Middle Europe [ME], Eastern Europe [EA], Northern Alps [NAL], Southern Alps [SAL], Iberian Peninsula [IP], Mediterranean region [MD], and North Africa [NA].

studies over Europe (Ban et al., 2021; Brogli et al., 2023; Cui et al., 2023; Leutwyler et al., 2017; Vergara-Temprado et al., 2021). In this study, we focus on the 2.2 km simulation, referred to as the COSMO simulation.

2.2. Hail and Lightning Diagnostics

The COSMO simulation is run with online hail and lightning diagnostics, using the same setup as described in Cui et al. (2023). For hail, we use the one-dimensional hail growth model CAM-HAILCAST (Adams-Selin & Ziegler, 2016), which simulates the maximum hail diameter at the ground. CAM-HAILCAST simulates the growth of hail embryos with initial diameters of 5, 7.5, and 10 mm during the adiabatic ascent of an air parcel based on the temperature, humidity, and pressure profile from the COSMO simulation. For simplicity, we use the term HAILCAST in the following, when referring to CAM-HAILCAST. The hail diagnostic is activated at each grid point every 5 min if the updraft velocity is larger than 10 m s^{-1} for more than 15 min. The HAILCAST output of maximum hail diameter is saved at a temporal resolution of 5 min. A post-processing step is required to eliminate spurious hail activation by HAILCAST. Since HAILCAST activation relies solely on updraft velocity, up-slope winds along steep topography can, on rare occasions, falsely trigger the activation of hail. To mitigate this, HAILCAST outputs that do not coincide with precipitation (available also every 5 min) in the surrounding area and time are filtered out, as hail is expected to occur in the vicinity of precipitation (Morgan et al., 1986). This method eliminates 4% of hail occurrences in winter and less than 1% during summer. Overall, the differences in the hail climatology are small between the raw and post-processed HAILCAST output. Further details of the post-processing steps are explained in Appendix A.

This HAILCAST setup has been validated in eight case studies over the Alpine-Adriatic region of severe convection showing that HAILCAST captures the main characteristic of the hail swaths well while underestimating the occurrence of extra-large hailstones, possibly due to an underestimation of updraft strength in a simulation with 2 km horizontal resolution (Cui et al., 2023). In this study, we further validate this HAILCAST setup focusing on the climatological scale.

For lightning, the LPI diagnostic (Brisson et al., 2021; Yair et al., 2010) is employed, which estimates the potential for charge generation and separation that leads to lightning strokes within the primary charging zone (0 and −20°C). LPI is based on the updraft velocity, which is scaled by the charge separation potential derived from the hydrometeor content. Spurious or unrealistic LPI signals due to weak, isolated updrafts and deep orographic gravity waves are filtered out. In our COSMO setup, LPI is calculated every 15 min of which the hourly maximum LPI is saved to the output.

2.3. Simulation Description and Analysis Domain

We conducted an 11-year COSMO simulation for the period 2011–2021. To ensure an adequate spin-up period, particularly for soil moisture, the outer 12 km domain was initialized in 2004, 7 years prior to the analysis period, using the 12 km soil moisture field from Vergara-Temprado et al. (2021) as initial conditions. The inner-domain, with a horizontal grid spacing of 2.2 km, was initialized on 19 October 2010, allowing for a spin-up period of 2.5 months, with outputs analyzed from 1 January 2011. Both domains encompass Europe between 10°W–25°E and 35°N–60°N using a rotated coordinate system. The 2.2 km domain employs a computational mesh of 1542 × 1542 grid points and a time step of 20 s. Maximum hail diameter and surface precipitation are stored every 5 min, whereas LPI and other variables are saved at a 1 hr resolution. A detailed list of the stored output variables is given in the Supporting Information (Tables S1 and S2 in Supporting Information S1).

The analysis is performed in predefined subdomains, depicted by the red boxes in Figure 1. These subdomains are adapted and extended from the Prediction of Regional scenarios and Uncertainties for Defining EuropeaN

Climate change risks and Effects (PRUDENCE) project (Christensen et al., 2007), to facilitate comparisons with previous regional climate modeling studies. The subdomains include the British Isles [BI], Baltic region [BA], France [FR], Middle Europe [ME], Eastern Europe [EA], Northern Alps [NAL], Southern Alps [SAL], Iberian Peninsula [IP], Mediterranean region [MD], and North Africa [NA]. For the Mediterranean region, the subdomain is further divided into land [MDL] and sea [MDS] regions, since the continent and the ocean exhibit different seasonal and diurnal cycles. For all other subdomains, only land grid points within the defined boxes in Figure 1 are included in the analysis.

2.4. Temperature and Precipitation Observations

Multiple observational data sets are used to validate precipitation, accounting for observational uncertainties and the large European domain.

The daily gridded observational data set E-OBS (v30.0e, Cornes et al., 2018), which is based on station data, provides daily precipitation and near-surface temperature fields at a horizontal resolution of 0.1° (approximately 10 km) for the entire time period of the COSMO simulation. For comparison of near-surface temperature, model output has been bilinearly remapped to the E-OBS grid and adjusted to account for topographical height differences between the model and E-OBS using a lapse rate of 0.65 K $(100\ \mathrm{m})^{-1}$ (following, e.g., Ban et al., 2014; Leutwyler et al., 2016).

The quality of the E-OBS data set varies across Europe and is biased in regions of low station density and, thus, shows too low precipitation amounts over the Alpine region compared to other data sets (Cornes et al., 2018; Isotta et al., 2014). To address this limitation, we further use the Alpine Precipitation Grid Data set (APGD) based on a high-resolution Alpine rain-gauge network with a lower uncertainty of the precipitation estimates due to higher station density. The APGD data set provides daily precipitation from 2011 to 2019 in the European Alps at a horizontal resolution of 5 km (Isotta et al., 2014).

In addition to in situ precipitation measurements, we use two remote-sensing data sets. The first is the European climatological high-resolution gauge-adjusted radar precipitation data set (EURADCLIM, Overeem et al., 2023) based on OPERA (Huuskonen et al., 2014). We use EURADCLIM with a temporal resolution of 1 hr and a horizontal resolution of 2 km, spanning the period from 2013 to 2021. The coverage of EURADCLIM depends on the data contributed to OPERA by the participating countries, which allows it to cover most of our analysis domain. However, this coverage excludes the Mediterranean Sea and several regions in Southern Europe. The EURADCLIM data set is used in the post-processing steps of the OPERA maximum reflectivity (see Section 2.5.1) and the validation of daily and hourly precipitation.

We also include the Integrated Multi-satellitE Retrievals for Global Precipitation Measurement (IMERG V07B, Huffman et al., 2023), which provides a rain-gauge adjusted satellite retrieval of surface precipitation. The IMERG data set is used at a horizontal resolution of 0.1° at a half-hourly time frequency. It encompasses our analysis domain, including seas and oceans that lack in situ precipitation measurements. We use the IMERG data set to analyze seasonal and diurnal cycles of precipitation from 2011 to 2021.

The fourth precipitation data set used is CombiPrecip (Germann et al., 2022; Sideris et al., 2014), which combines radar data with automated rain-gauge measurements across Switzerland. CombiPrecip provides a high-resolution data set with an hourly temporal resolution and a horizontal resolution of 1 km, providing detailed information about precipitation patterns over the Swiss Alps. This data set will be used to validate simulated hourly heavy precipitation events.

2.5. Hail Observations

2.5.1. Radar-Based Hail Detection Algorithms

Two radar-based hail detection algorithms are used to validate the COSMO hail climatology: one from an existing data set over the Alpine region and a newly derived European-wide data set.

The probability of hail (POH, Waldvogel et al., 1979) product is based on the MeteoSwiss network of C-band Doppler radars (Germann et al., 2015; Trefalt et al., 2023). It is available with a spatial resolution of 1 km and a temporal resolution of 5 min. POH provides a probabilistic estimate of the presence of hail of any size at the ground, and is calculated based on the vertical distance between the 45 dBZ radar echo top height and the freezing

level height extracted from COSMO (Waldvogel et al., 1979; Witt et al., 1998). The first hail climatology for the Alpine region using POH was developed by Nisi et al. (2016). POH has been evaluated against insurance car damage data (Nisi et al., 2016) and crowd-sourced reports (Barras et al., 2019), showing that a threshold of POH>80% adequately identifies hail regions. POH is used here in the Alpine domain covered by the MeteoSwiss radar network from 2011 to 2021.

To further evaluate the models' performance across Europe, we construct a European-wide proxy of hail occurrence using the 2D maximum radar reflectivity from the OPERA composite. OPERA provides post-processed radar reflectivity covering most of the continental regions within the domain of our COSMO simulations. However, many radar clutter pixels remain in the data and have to be filtered out. The filtering process involves five steps, first smaller-scale clutter is filtered out in steps (a)–(c), followed by larger-scale criteria in steps (d) and (e) (schematic flowchart provided in Figure S4 in Supporting Information S1): (a) We remove clutter from the OPERA radar data using the filter by Gabella and Notarpietro (2002). (b) Reflectivity values larger than 60 dBZ that persist only for one time step of 15 min are removed. (c) We filter out stationary non-meteorological echoes if the reflectivity value is larger than 50 dBZ and remains constant (i.e., changes less than or equal to 0.5 dBZ) for three consecutive time steps at the same grid point. (d) High reflectivity values larger than 50 dBZ are removed if hourly precipitation, based on EURADCLIM, at the same grid point is smaller than 10 mm. (e) A lightning filter is applied using ATDnet lightning observations to remove the remaining erroneous signals in the radar data, similar to Fluck et al. (2021). High reflectivity values larger than 50 dBZ are removed if no lightning occurred within a radius of 10 km in a 24 hr time window. This filtered OPERA reflectivity data set is then used to derive a proxy for whether hail occurred or not, hereafter named EURADHAIL, by defining a reflectivity threshold based on a comparison with POH over the Alpine region, see Section 2.7. This data set with binary mask (0 or 1) has a horizontal resolution of 2 km and a temporal resolution of 1 hr, available for the years 2013–2021 for evaluation. Details on the OPERA radar locations (2013–2021) are available in Figure S5 in Supporting Information S1, and quality checks evaluating the distribution reflectivity of various radar types are provided in Figure S6 in Supporting Information S1.

The main difference between the POH and EURADHAIL data sets is the vertical extent of information utilized. POH is based on 3D radar reflectivity, which also incorporates the freezing level height, providing a more comprehensive picture of hail formation. In contrast, EURADHAIL relies on 2D radar reflectivity, lacking information on the storm's vertical structure. Although EURADHAIL detects high radar reflectivity values often associated with hail, it cannot determine whether this reflectivity extends vertically above the freezing level height—an important indicator for determining actual hail intensity. Additionally, its reliance on 2D reflectivity means it may also detect heavy precipitation events that are not necessarily hail-related, despite the use of lighting observations to filter out some non-hail cases. Similarly, the absence of high reflectivity does not necessarily rule out the occurrence of hail. Furthermore, due to an increase in the number of radars contributing to the OPERA data set, the spatial coverage of EURADHAIL changes with time. These limitations highlight that EURADHAIL should be interpreted as a best-effort estimate of hail occurrence rather than a definitive hail product. Users should be mindful of these constraints when interpreting hail occurrence using the EURADHAIL proxy.

2.5.2. Crowd-Sourced ESWD Data Set

As direct European-wide hail observations, we use the quality-controlled severe weather reports operated by the European Severe Weather Database (ESWD, European Weather Observer https://www.eswd.eu/ESWD/, Dotzek et al., 2009), which was established in 2006 by the European Severe Storms Laboratory. We are using ESWD crowd-sourced reports of large hail from 2011 to 2021, gridded to the OPERA horizontal grid with approximately 2 km grid spacing. Large hail is defined as hailstones with a diameter exceeding 20 mm or as a layer of hail on a flat surface thicker than 20 mm.

Crowd-sourced reports have inherent limitations, such as spatial variations in reporting efficiency, biases related to population density, and increasing report rates in recent years, all of which contribute to spatial and temporal inconsistencies. For instance, the ESWD shows a reporting bias toward central Europe (Hulton & Schultz, 2024; Taszarek et al., 2019). To cope with this issue, we concentrate our comparison on the seasonal and diurnal cycle of hail reports for each grid cell. These measures can be considered as robust and not too strongly affected by the aforementioned issues.

2.5.3. Hailpad and Drone-Based Photogrammetry Data Sets

For the evaluation of time-aggregated hail size distributions, we use a hailpad data set over the plain of Friuli Venezia Giulia (FVG), situated over the north-easternmost part of Italy (Manzato, Cicogna, et al., 2022). This network is coordinated by the regional meteorological service Osservatorio Meteorologico Regionale (OSMER) and Restione Rischi Naturali (GRN)–Agenzia Regionale per la Protezione dell'Ambiente (ARPA FVG–OSMER, 2021) and in operation since 1988. We analyze the daily hail database of four macro-areas from April–September between 1988 and 2016, where the daily maximum hail diameter is defined as the largest recorded diameter among all hailpads on a given day.

We further use drone-based surveys of hailstones from Argentina (Soderholm et al., 2020) and Switzerland (Lainer et al., 2024). Following the HailPixel procedure by Soderholm et al. (2020), these data sets are based on a machine learning technique to detect hailstones from drone images. Each data set provides the hail size distribution from a single hail event, where the drone surveyed an area of approximately 1000 m^2.

2.6. Lightning Observations

For the validation of simulated lightning, we use the ATDnet network operated by the UK Met Office, which is a very low-frequency long-range lightning location system (Anderson & Klugmann, 2014). It detects lightning by measuring the electromagnetic fields generated by lightning discharges and determining the location using the time difference information from multiple antennas. The long-range detection system can observe lightning in remote areas and over bodies of water. However, it has larger location errors compared to short-range systems. In three case studies over the Mediterranean Sea, the ATDnet data set has been estimated to detect 89% of all cloud-to-ground flashes and 24% of all in-cloud flashes (Enno et al., 2016). Over Belgium, a flash detection efficiency of 88% has been found, whereas the stroke detection efficiency varied between 23% and 75% (Poelman et al., 2013). These findings indicate that ATDnet can miss single lightning strokes but overall catches most of the lightning flashes. Similar results are expected over central Europe with an ATDnet location accuracy of 1–2 km over western Europe and 5–10 km over the remaining region, which extends between Helsinki (Finland), Valentia (Ireland), Gibraltar, and Cyprus (Enno et al., 2020). The location accuracy of ATDnet of a few kilometers is lower compared to other lightning data sets, which can have a location accuracy up to a few 100 m (Betz et al., 2009; Schulz et al., 2005), but it is sufficient for the evaluation of the COSMO simulation with a similar horizontal resolution. Even though the ATDnet data set undercatches weak in-cloud flashes, we believe that this data set serves the purpose of our study to compare climatological daily lightning frequencies over a large area. In this study, we use the number of ATDnet lightning strokes from 2011 to 2021 in our analysis domain on a grid with 2 km horizontal grid spacing to calibrate the COSMO LPI output and compare spatial and temporal patterns of lightning activity over Europe.

2.7. Evaluation Approach

In the following section, we describe the methods used to calculate indices and variables for comparing the modeled and observed data sets.

2.7.1. Precipitation Indices

For the validation of modeled surface precipitation, we evaluate the mean precipitation, the wet day frequency, wet day intensity, and heavy precipitation. A wet day is defined as a day with precipitation $\geq$1 mm. Daily precipitation is considered as heavy if it exceeds the daily 99th percentile (p99D), for hourly precipitation if it exceeds the hourly 99.9th percentile (p99.9H) following Schär et al. (2016).

2.7.2. Definition of Hail Days, Hail Size Categories, and Data Aggregation Approach

The hail data sets used in this study describe hail occurrence in various ways. The HAILCAST output from COSMO provides the maximum hailstone diameter in the last 5 min, the ESWD reports mostly large hailstones with diameters larger than 20 mm, the radar-derived product POH indicates the probability of hail, and EUR-ADHAIL gives categorical information on whether hail occurred within the last 15 min or not. To facilitate comparisons between the data sets, each hail variable is converted to the number of hail days or hail hours. The 24 hr between 06 UTC and 06 UTC of the following day are considered for each day, taking into account the

minimum hail activity in the early morning hours. This allows the best possible separation of independent hail events.

For ESWD, a hail hour or hail day occurs if there is at least one hail report for the time period of interest. For POH, a hail day occurs for POH>80%, following Nisi et al. (2016). For HAILCAST and EURADHAIL, a threshold in hail diameter or radar reflectivity, respectively, has to be defined. In a sensitivity experiment, the hail day frequency for different thresholds of hail diameter and radar reflectivity, respectively, are compared to the hail day frequency based on POH. This analysis is done for the Alpine domain of the POH data and the full time period of the simulation. The lowest root-mean-square deviation of hail days between HAILCAST and POH can be found for a hail diameter threshold of 12.5 mm (Figure S7 in Supporting Information S1). We therefore use a threshold of 12.5 mm to calculate hail days and hail hours based on the HAILCAST output. For EURADHAIL, the optimal radar reflectivity threshold based on the root-mean-square deviation with POH hail days over Switzerland is 53 dBZ (Figure S7 in Supporting Information S1), which is similar to values of 55 dBZ reported in previous studies (e.g., Fluck et al., 2021; Kunz & Kugel, 2015; Schiesser, 1990).

For the comparison of hail peak hours and months, we aggregate the hail occurrence to a coarser resolution. This aggregation smoothes the fields to improve comparability. The hail frequency is aggregated to a 30 km spatial resolution following a symmetric extremal dependence index analysis (SEDI, Ferro & Stephenson, 2011) of daily hail day occurrence in COSMO and EURADHAIL. With a resolution of 30 km, the mean daily SEDI of COSMO is larger than 0.5 during 2011–2021 compared to EURADHAIL, indicating improved agreement between at this resolution (not shown).

2.7.3. Adjustment of LPI to Lightning Stroke Density

Considering that LPI only provides the potential of lightning, it has to be calibrated by observations to estimate the number of lightning strokes (Brisson et al., 2021). We utilize quantile mapping to get the lightning stroke density from LPI, whereby the simulated distribution of lightning strokes is aligned with the observed lightning stroke density from ATDnet (see Figure S10 in Supporting Information S1). By definition, this method leads to a close agreement in the total number of lightning strokes between ATDnet and in the post-processed COSMO output while allowing for different spatial and temporal patterns. The evaluation of the COSMO lightning climatology will therefore focus on the spatial and temporal patterns of lightning occurrence over Europe. We consider a lightning day (or lightning hour) per grid box if the number of strokes in the considered period exceeds 2 to reduce the influence of spurious stroke signals. Similar to hail, a lightning day is defined from 06 UTC to 06 UTC of the following day.

3. Evaluation of Simulated Surface Temperature and Precipitation

In the first step, we compare the model output fields of surface temperature and precipitation against observations. Both variables are evaluated for multi-year mean fields across seasons—spring (MAM), summer (JJA), autumn (SON), and winter (DJF). Additionally, for precipitation, several indices, as well as the seasonal and diurnal cycles are validated. The validation of temperature and precipitation will consider the ability of the COSMO model to simulate the climatic conditions across Europe. For consistency and comparability, this assessment uses similar fields (e.g., precipitation indices) as previous studies (e.g., Ban et al., 2014; Leutwyler et al., 2017; Vergara-Temprado et al., 2021).

3.1. Temperature

The bias in modeled 2 m temperature over the European continent is generally small, with most regions showing a cold bias of less than 2°C for all seasons (Figure 2). It is worth noting that the JJA and DJF biases are much improved in comparison to previous simulations. This is particularly important in JJA when temperature biases were previously larger than 2.5°C in large portions of eastern Europe (Leutwyler et al., 2017; Pham et al., 2021). One of the reasons for improved temperature fields in our simulation might be improvements in ERA5 temperatures compared to its predecessor ERA-Interim (Hersbach et al., 2020), which was used as boundary and initial data in Leutwyler et al. (2017) and Pham et al. (2021). Over the Iberian Peninsula, the model shows a larger cold bias than in the remaining domain, but still within a range of −2°C, similar to previous studies (Kotlarski et al., 2014; Pham et al., 2021). Large discrepancies in 2 m temperature are evident over North Africa, a known

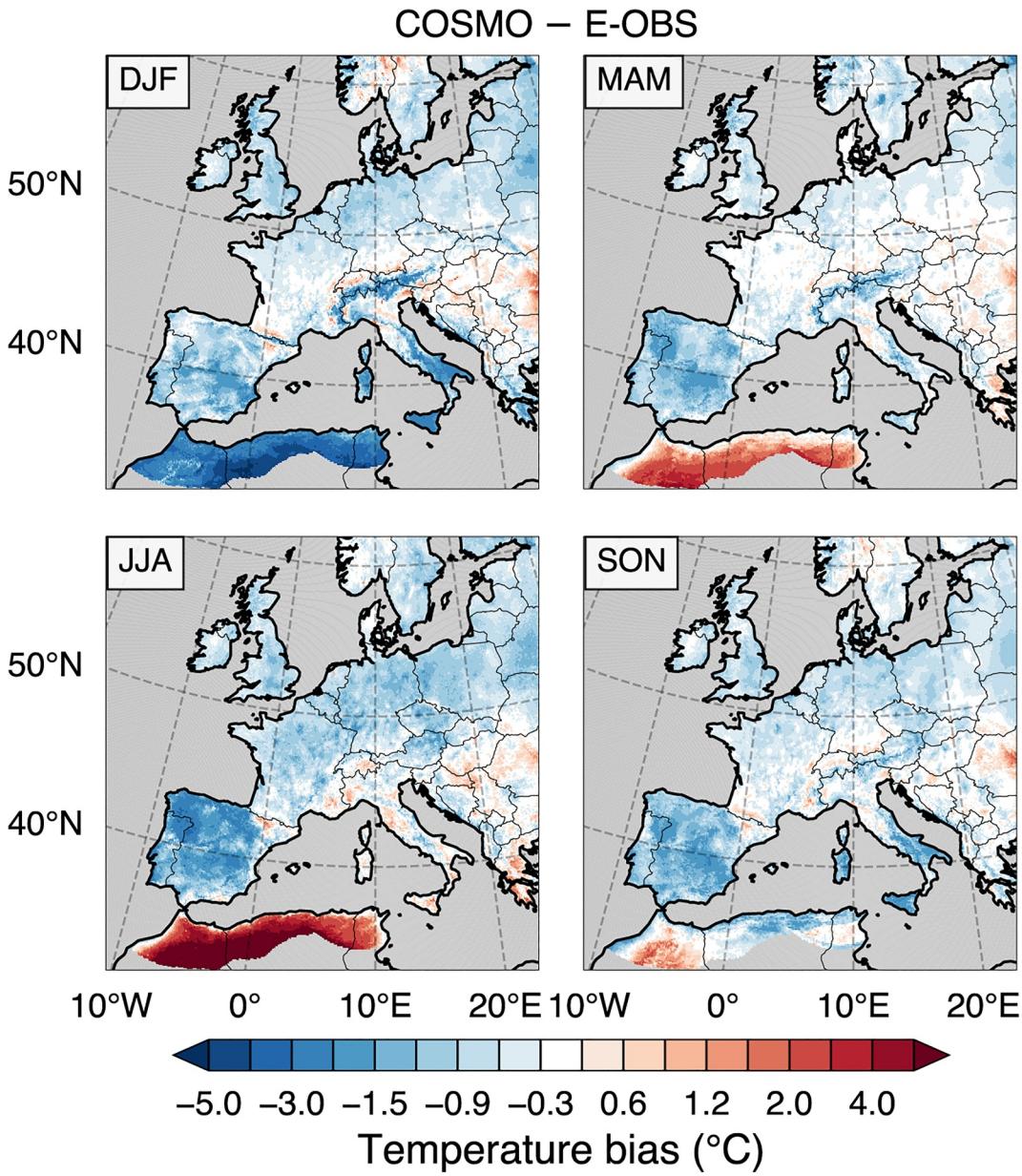

Figure 2. Seasonal-mean 2 m temperature bias of COSMO with respect to E-OBS for winter (DJF), spring (MAM), summer (JJA), and autumn (SON) for the years 2011–2021. To account for elevation differences between the model and observation, a height correction was applied using a lapse rate of 0.65 K (100 m)$^{-1}$.

issue due to the scarcity of stations in this region incorporated in E-OBS, as well as considerable uncertainties associated with the interpolation process (Cornes et al., 2018; Kotlarski et al., 2014; Panitz et al., 2014).

3.2. Precipitation

3.2.1. Spatial Patterns

Daily accumulated precipitation fields during summer (JJA) are compared against several observational data sets: radar-based EURADCLIM, rain-gauge based E-OBS and APGD, and satellite-based IMERG (Figure 3). ERA5 precipitation is also included for reference. All precipitation observations are shown in their native spatial resolution for visualization. The spatial comparison focuses on summer, which is the main convective season for most regions in Europe (Taszarek et al., 2020), with analyses for other seasons available in Figures S1–S3 in

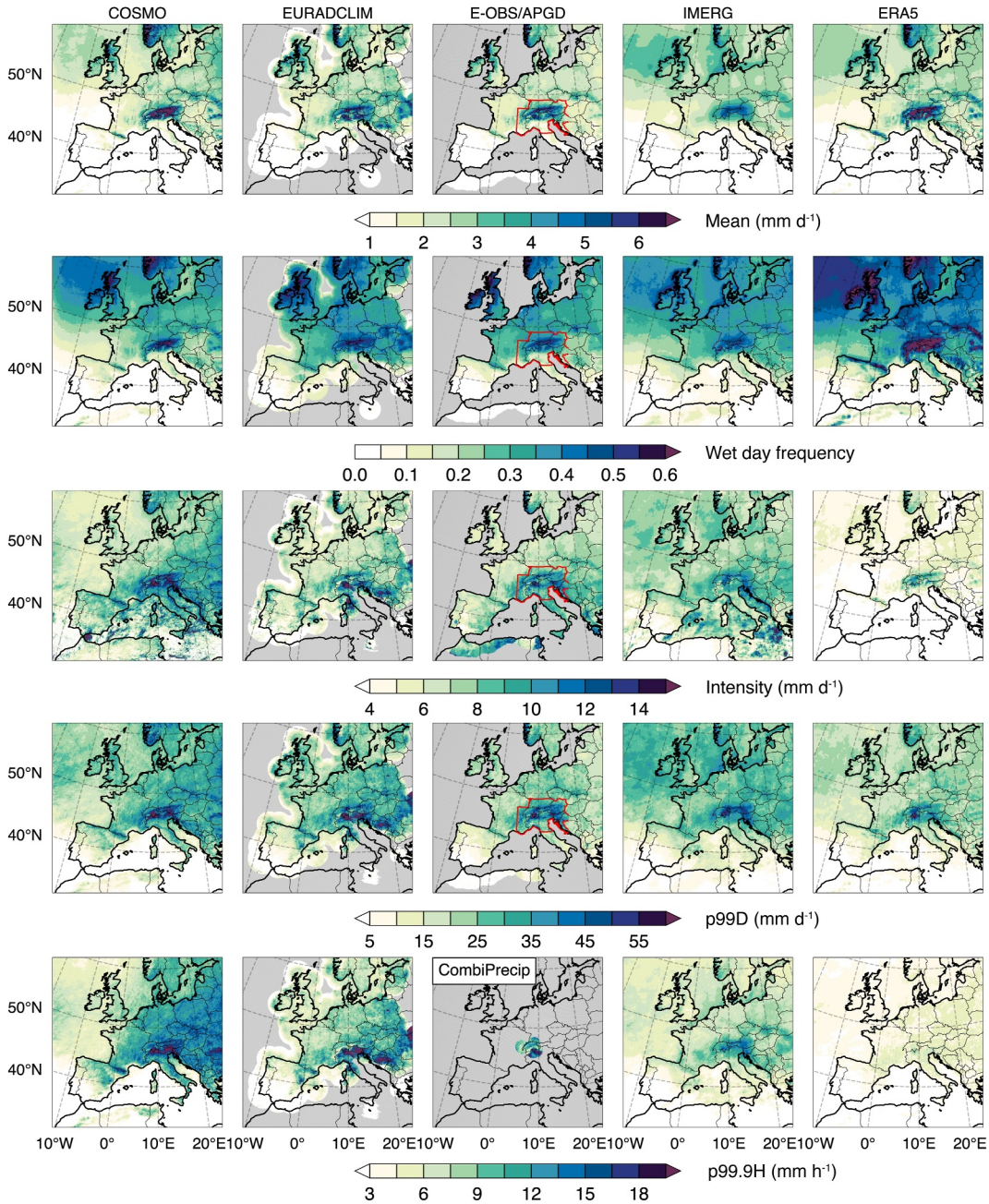

Figure 3. Validation of summer (JJA) surface precipitation. From top to bottom are shown: mean daily precipitation, wet day frequency of precipitation >1 mm day^{-1}, mean intensity of precipitation >1 mm day^{-1}, the 99th percentile of daily accumulated precipitation, and the 99.9th percentile of hourly accumulated precipitation. The columns show, from left to right, COSMO, the observational data sets EURADCLIM, E-OBS/APGD, and IMERG, and ERA5 reanalysis. Due to data availability, EURADCLIM is shown for 2013–2021 only. For E-OBS/APGD, heavy precipitation is only presented on the daily timescale, with APGD shown in the Alpine region (red outline) for 2011–2019. In the last row, the 99.9th percentile of hourly precipitation based on CombiPrecip is shown for 2011–2021.

Supporting Information S1. The COSMO simulation produces mean precipitation patterns similar to those in ERA5, which serves as the boundary conditions for the simulation. Qualitatively, COSMO mean precipitation aligns well with observations, capturing key features such as maxima over the Alpine ridge, the Norwegian coast, the British Isles, and the Carpathian Mountains (first row in Figure 3).

In terms of wet day frequency and intensity, COSMO demonstrates good agreement with EURADCLIM, APGD, and IMERG (second and third rows in Figure 3). Compared to observational data sets, ERA5 tends to overestimate wet day frequency and underestimate precipitation intensity, particularly for events with precipitation exceeding 10 mm hr^{-1} (Lombardo & Bitting, 2024). This bias has been documented in many studies across Europe. IMERG, on the other hand, underestimates both wet day frequency and intensity over the Alps compared to APGD and EURADCLIM, likely due to its underestimation of daily maximum precipitation in mountainous regions (O & Kirstetter, 2018).

COSMO shows an overestimation of heavy precipitation, both on the daily and hourly timescale, across the entire domain compared to E-OBS and APGD, though it agrees well with EURADCLIM (fourth and fifth rows in Figure 3). This discrepancy may result from the undercatchment of precipitation by rain gauges, caused by flow distortion around gauges, and/or undersampling due to the limited number of gauges (Isotta et al., 2014).

3.2.2. Seasonal and Diurnal Cycles

We compare the modeled seasonal and diurnal cycles of heavy precipitation to IMERG observations, which has the best spatial coverage of the observational data sets while also adequately representing heavy precipitation (compare Figure 3). The seasonal cycle of heavy precipitation (99th percentile of daily precipitation) differs strongly across the subdomains defined in Figure 1. In the subdomains EA and ME, the peak occurs in summer, whereas SAL, IP, MD, and NA experience the highest occurrence of heavy precipitation in autumn (top row in Figure 4). The model captures these peaks in the seasonal cycle well. The subdomains NAL, FR and BI display less distinct peaks in the simulation and observations. Notably, the largest differences between the model and observations are found in NAL, where the observations show a second precipitation peak in autumn, similar to SAL, which is absent in the COSMO simulation. During autumn, upper-level troughs frequently cause strong airflows toward the Alps, which can lead to heavy precipitation and trigger severe floods along the Southern Alps (e.g., Doswell et al., 1998; Massacand et al., 1998; Rotunno & Houze, 2007; Sénési et al., 1996). If the upper-level trough reaches the Mediterranean further east, then heavy precipitation can occur in NAL instead of SAL, most likely leading to the observed autumn peak of heavy precipitation in NAL. An example of such an event was discussed by Piaget et al. (2015). It appears that the intensity of this type of event is underestimated in the COSMO simulations.

To assess the diurnal cycle of precipitation in summertime convective systems, when we expect hail formation, we focus on the period from April to September, when most convective events across Europe are expected to occur (Punge & Kunz, 2016), to evaluate the diurnal cycle of heavy precipitation in our simulation. During these six months, the diurnal cycle of heavy precipitation shows peak frequencies of heavy precipitation between 14 and 16 UTC in both the model and observations in all subdomains, with the exception of BI, BA, and MDS (top row in Figure 5). The modeled afternoon peak is particularly pronounced in NAL, SAL, and EA, whereas the observations indicate a weaker peak at a slightly later time. These overly pronounced peaks in modeled heavy precipitation across many subdomains reflect, on the one hand, the simulation's tendency to overestimate heavy precipitation, a finding consistent with previous studies (Ban et al., 2015; Leutwyler et al., 2017). On the other hand, IMERG, which is a combined product of satellite remote sensing and station data, is known to underestimate precipitation over mountainous, that is, in under-sampled regions (O & Kirstetter, 2018), which can further increase the discrepancies between the model and observations. The British Isles show no pronounced peak in daily precipitation, highlighting the importance of large-scale forced, day-time independent precipitation in the eastern North Atlantic. In the Mediterranean, the model indicates a peak in heavy precipitation between 12 and 13 UTC, with a weaker secondary peak in the early morning at 04 UTC. This early morning peak is also observed in measurements and reflects the frequent development of convective precipitation over the Mediterranean Sea after midnight. In contrast to COSMO, IMERG shows a pronounced early morning peak in the observations for many subdomains. A comparison of the diurnal cycles of ERA5, IMERG, and EURADCLIM showed that these early morning peaks are only visible in the IMERG data set (not shown), indicating that IMERG might overestimate this morning peak in heavy precipitation. However, previous studies have shown that COSMO-CLM simulations were unable to reproduce early morning hail or lightning events over and around the Adriatic Sea (Cui et al., 2023; Malečić et al., 2022). Thus, this discrepancy in the diurnal cycle between COSMO and IMERG might be a combined effect of an under- and overestimation of early morning in COSMO and IMERG, respectively.

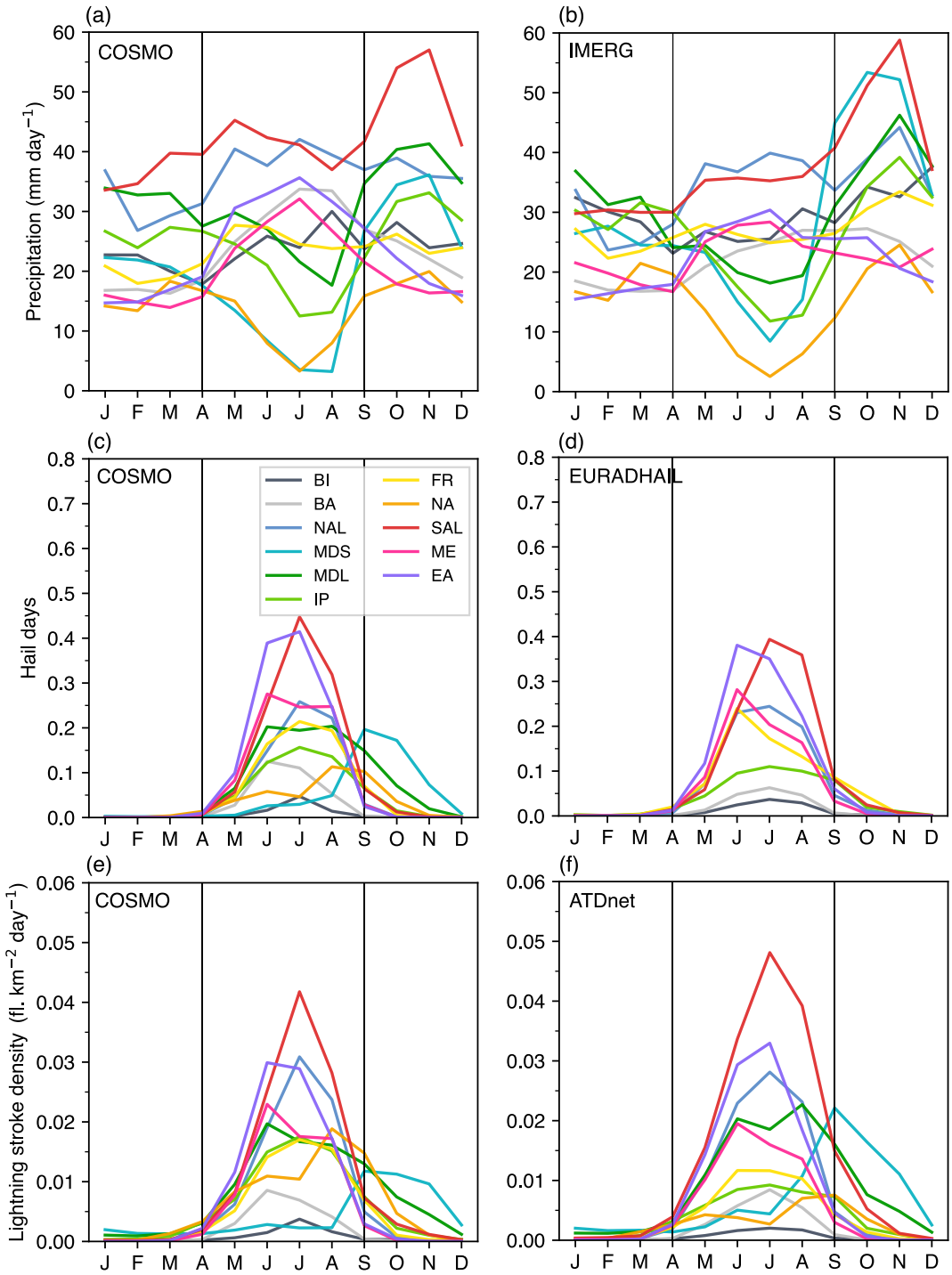

Figure 4. Seasonal cycles in different subdomains (see Figure 1) of (a, b) heavy precipitation (p99D), (c, d) hail days, and (e, f) lightning stroke density from (left panels) COSMO and (right panels) observations from EURADHAIL (2013–2021), ATDnet, and IMERG, respectively, during 2011–2021. Note that due to low data quality and coverage, no EURADHAIL data are shown for MDS, MDL, and NA. All subdomains, except MDS, focus exclusively on land.

In summary, the comparison of surface temperature and precipitation between the COSMO simulation and observations indicates that COSMO accurately captures climatic conditions over Europe, also during the convective seasons. This good performance suggests that COSMO provides a reliable climatological representation of convective activity, which can be further evaluated using hail and lightning diagnostics in the next Sections.

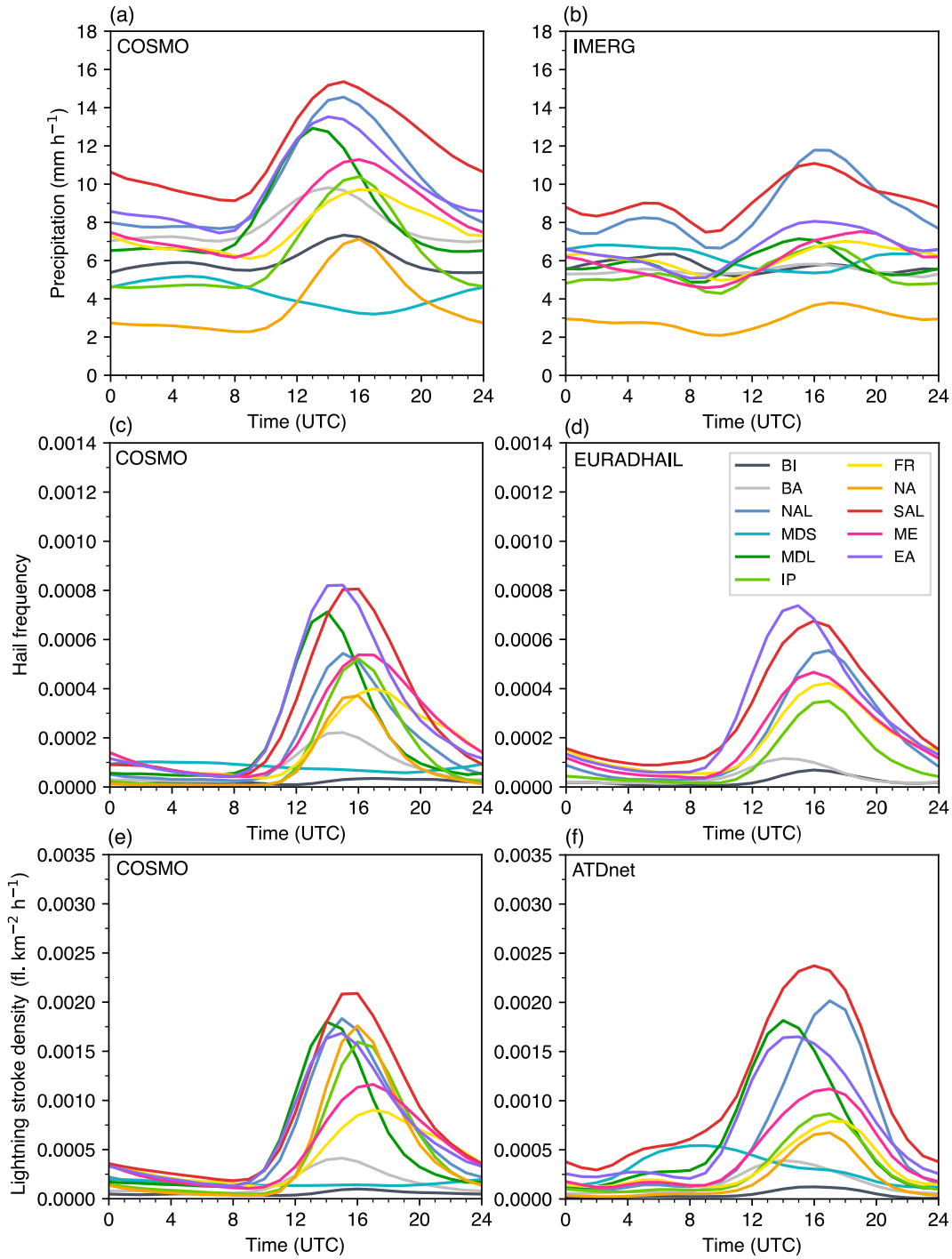

Figure 5. Diurnal cycles in different subdomains of (a, b) heavy precipitation (p99.9H), (c, d) hail frequency, and (e, f) lightning stroke density from (left panels) COSMO and (right panels) observations from EURADHAIL (2013–2021), ATDnet, and IMERG, respectively, from April to September for 2011–2021. Again, due to low data quality and coverage, no EURADHAIL data are shown for MDS, MDL, and NA. All subdomains, except MDS, focus exclusively on land.

4. European Hail Climatology

The assessment of hail occurrence in COSMO is based on the comparison of the number of hail days (see definitions in Section 2.5) between the simulation and observations. This comparison is carried out in four steps: (a) over the full European model domain using EURADHAIL, (b) over the western to central Alpine domain using

EURADHAIL and POH, (c) by comparing the interannual variability of the number of hail days, and (d) by analyzing seasonal and diurnal cycles in specific subdomains. This section concludes with a discussion of the hail size distribution simulated by HAILCAST in COSMO, followed by a comparison with findings from previous studies.

4.1. Spatial Distribution Over Europe

A comparison between COSMO and EURADHAIL hail days reveals similar monthly patterns of hail occurrence throughout the convective season (Figure 6). The hail activity in Europe typically begins in May, when most regions experience fewer than 0.2 hail days per month, that is, in May around one hail day occurs every 5 years. An exception is the area around the Carpathian Mountains, where up to 0.6 hail days per month are observed in EURADHAIL. During the summer months, the number of hail days increases across continental Europe in both data sets. The highest hail frequencies in COSMO are found in eastern Europe and the Po Valley, with values up to 1.5 hail days in northern Italy in July. Although COSMO shows higher values in the Po Valley than EURADHAIL, this discrepancy likely results from beam blockage along the Alps and insufficient data availability in large parts of Italy in the OPERA composite. In eastern Europe, COSMO shows more hail days in the north (e.g., Poland), whereas values further south align closely with EURADHAIL. Particularly for the hail hotspots in eastern Austria, Slovenia, and western Ukraine, the model and observations are in good agreement. Along the coasts of France and Spain, the hail day frequencies agree well between the two data sets, with slightly higher values around the Massif Central in EURADHAIL. In autumn, the number of hail days decreases across continental Europe but increases over the Mediterranean Sea in both data sets. However, the sparse radar coverage over the Mediterranean makes comparisons challenging. Hail activity largely ceases over the sea by November in COSMO (see Figure S8 in Supporting Information S1).

The higher frequency of hail days over northeastern Europe in COSMO compared to EURADHAIL is similar to the pattern for heavy precipitation during the summer months (Figure 3), particularly at the hourly timescale, where COSMO shows higher heavy precipitation values in northern Europe than EURADCLIM. Several reasons could lead to this discrepancy. On the one hand, radar coverage in the OPERA network is scarce along the eastern Baltic Sea, which might lead to a low bias in EURADCLIM and EURADHAIL. On the other hand, a higher number of hail days in northern Europe in COSMO could be attributed to the model's tendency to overestimate convection and convective updrafts in these regions.

The comparison of COSMO and EURADHAIL hail days across Europe showed that both data sets similarly represent the spatial distribution of hail occurrence, with the highest values near steep topography during the summer months. However, there are some differences, particularly in the precise locations of maximum hail activity along these mountain ranges. For a more detailed comparison of hail occurrence in regions with complex topography, COSMO hail days will be compared with hail days derived from POH and EURADHAIL over the Alpine region.

4.2. Spatial Distribution Over the Alpine Region

Validating hail days over the western to central Alpine domain allows us to assess the model performance in the hail-prone northern and southern pre-Alps at high spatial resolution. As depicted in Figure 7, the monthly hail days agree well between the COSMO model and POH, with the highest frequencies (>1.5 hail days month^{-1}) in the Po Valley from June to August. In EURADHAIL, some clutter remains along the southern pre-Alps after the filtering. Together with a gap in the OPERA radar coverage in Italy, a comparison of hail days in the Po Valley region of EURADHAIL with POH and COSMO is not possible. North of the Alps, similar hail day hotspots can be identified in POH and EURADHAIL along the northern Swiss pre-Alps and Jura Mountains, with slightly lower values in EURADHAIL than POH. Although POH and EURADHAIL observations show distinct hotspots of hail occurrence north of the Alps, with up to 1 hail day month^{-1}, these hotspots are less pronounced and localized in the COSMO simulation. However, the COSMO model shows elevated hail frequencies along the northern pre-Alps during the summer months compared to spring and autumn, and the month-to-month differences in hail occurrence are remarkably well represented. Orographic forcing is known to play a crucial role in initiating convection in the northern Swiss pre-Alps (Huntrieser et al., 1997; van Delden, 2001). Even though the COSMO simulation, with a 2.2 km grid spacing, represents the Alpine topography in considerable detail, it still

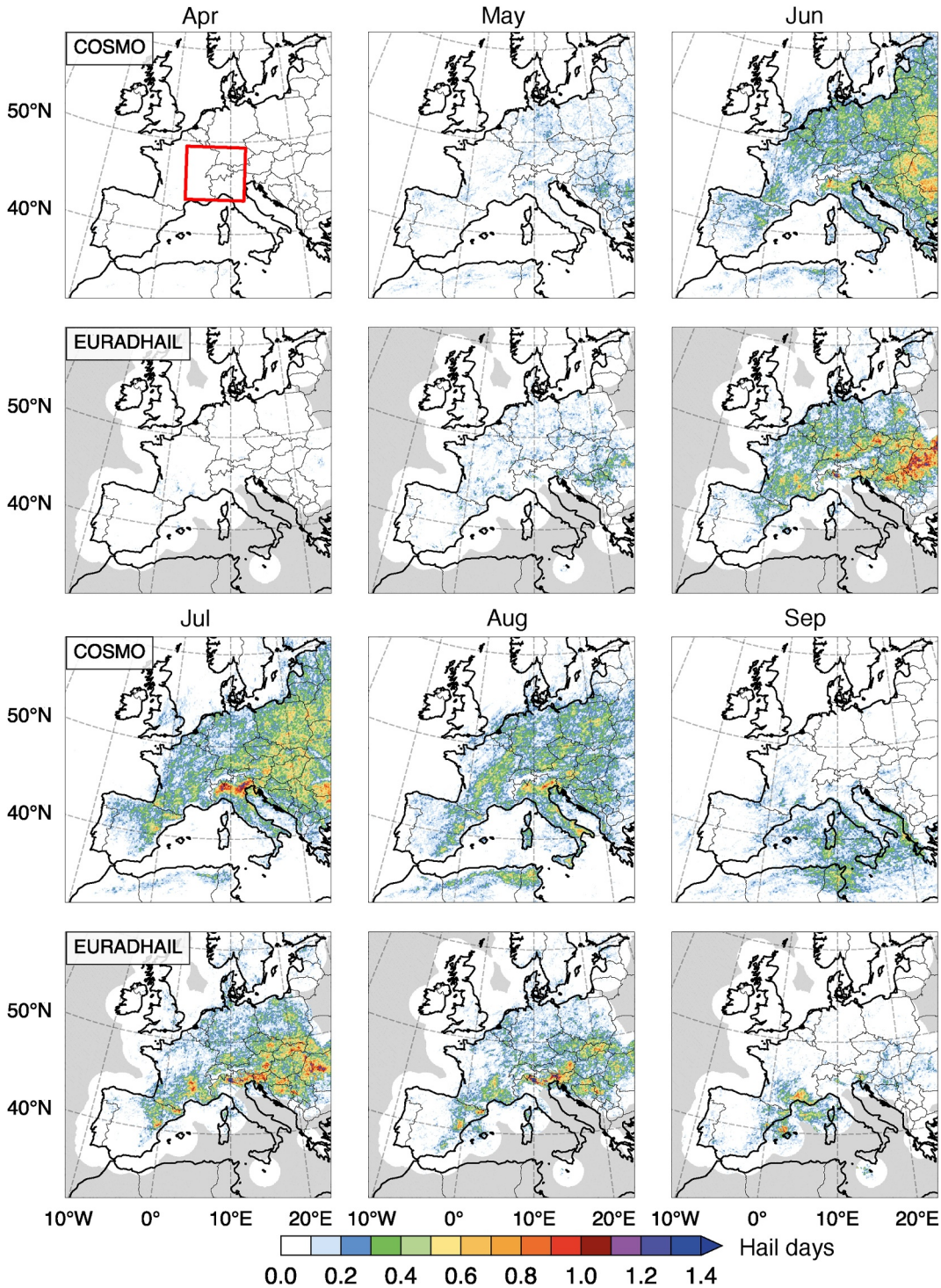

Figure 6. Monthly mean hail days from COSMO (hail diameter from HAILCAST ≥ 12.5 mm, 2011–2021) and EURADHAIL (2013–2021) from April to September. The red box represents the zoomed-in domain covered by the Swiss radar network shown in Figure 7. All data sets are shown at a spatial resolution of 2.2 km with 1.5σ Gaussian smoothing applied spatially.

misses small-scale orographic features that are important for initiating convection and the downstream development of hail. This limitation could result in a less localized hail occurrence over the northern Swiss pre-Alps in the simulation compared to observations.

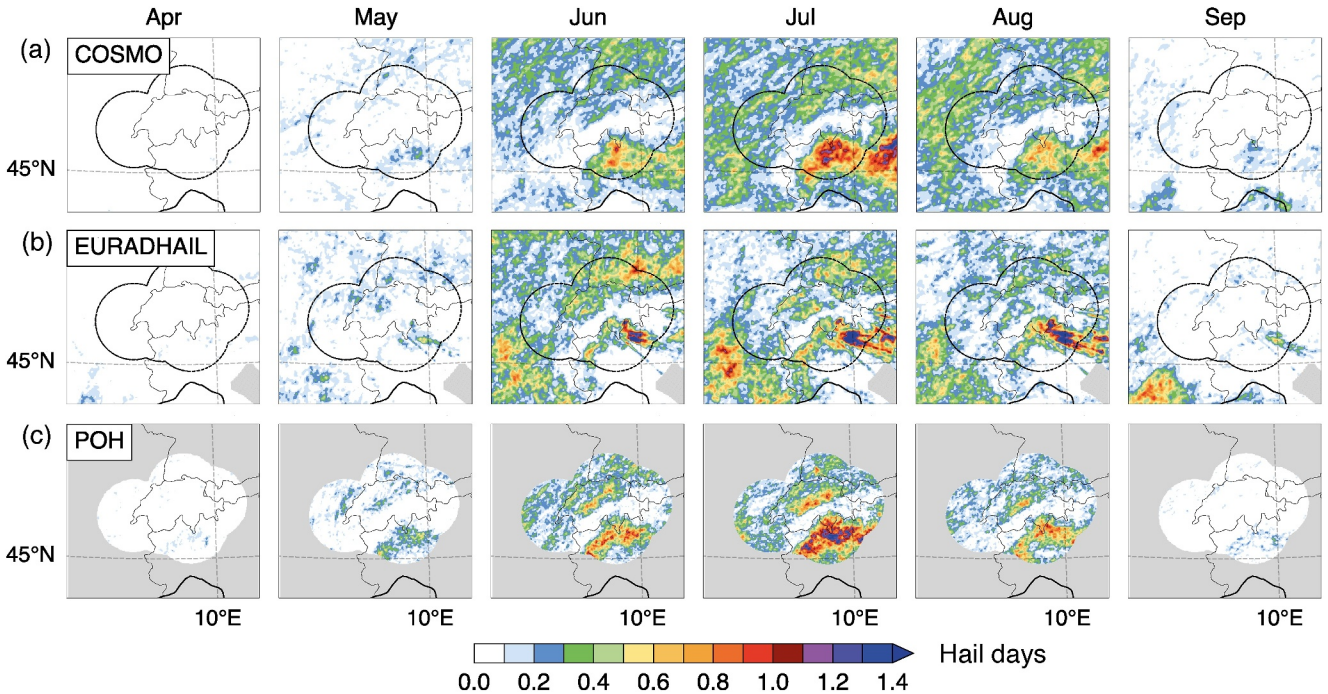

Figure 7. Monthly mean hail days from (a) COSMO (hail diameter from HAILCAST ≥ 12.5 mm, 2011–2021), (b) EURADHAIL (maximum reflectivity within the column ≥ 53 dBZ, 2013–2021), and (c) radar-based observations (POH ≥ 80%) from April to September. COSMO and EURADHAIL are shown at a spatial resolution of 2.2 km, POH at a spatial resolution of 1 km with 1.5σ Gaussian smoothing applied spatially.

4.3. Interannual Variations

Figure 8 shows the interannual variation of hail and lightning days from COSMO and observations. Over the period 2011–2021, the mean number of hail days across the subdomains ranged between 0 and 2 days. The hail days over the whole analysis domain show a local minimum in 2015 or 2016 for COSMO, which is also observed from stations in Croatia (Blašković et al., 2023; Jelić et al., 2020) and consistent with the lightning days in COSMO and ATDnet. A prominent feature is the peak in hail activity in 2018 for most of the domain, likely related to the 2018 European heat wave (Rösner et al., 2019). The variability of hail days over the British Isles in COSMO is consistent with Wells et al. (2024) with peaks in 2014, 2016 and 2019. The EURADHAIL proxy shows an overall increase in hail days for most subdomains after 2015. This increase is a result of the increasing number of radars contributing to the OPERA composite until 2018 (Overeem et al., 2023, also in Figure S6 in Supporting Information S1). The correlation between the interannual COSMO and EURADHAIL hail day frequency is weak for many subdomains resulting from this increase in OPERA radar coverage over time (see Table S1 in Supporting Information S1). Prominently, the interannual frequencies of COSMO and EURADHAIL anti-correlate for the subdomains FR and ME. These regions experienced a strong quality increase in the OPERA data set between 2012 and 2018 (Saltikoff et al., 2019), possibly causing unexpected interannual frequency changes. Nonetheless, the prominent peak in hail and lightning activity in 2018 is also visible in the EURADHAIL data set. This suggests that the EURADHAIL data set is more reliable in recent years. Although COSMO hail days do not correlate well with EURADHAIL, they correlate well with lightning days in ATDnet (with a mean Pearson's correlation coefficient over the model domain of 0.7, compare Table S1 in Supporting Information S1). An outlier is the EA subdomain that shows a low correlation between COSMO and ATDnet due to different occurrence frequencies at the beginning and end of the simulated time window. This might be related to less co-location of hail and lightning in convection systems in this region, or possibly a dominant role of meso-scale processes for the convection initiation in this region, providing only weak constraints for modeling interannual variability at the domain boundaries. The generally good agreement in terms of Pearson's correlation shows that COSMO successfully simulates the interannual variability of the occurrence of convective systems over Europe and in the subdomains.

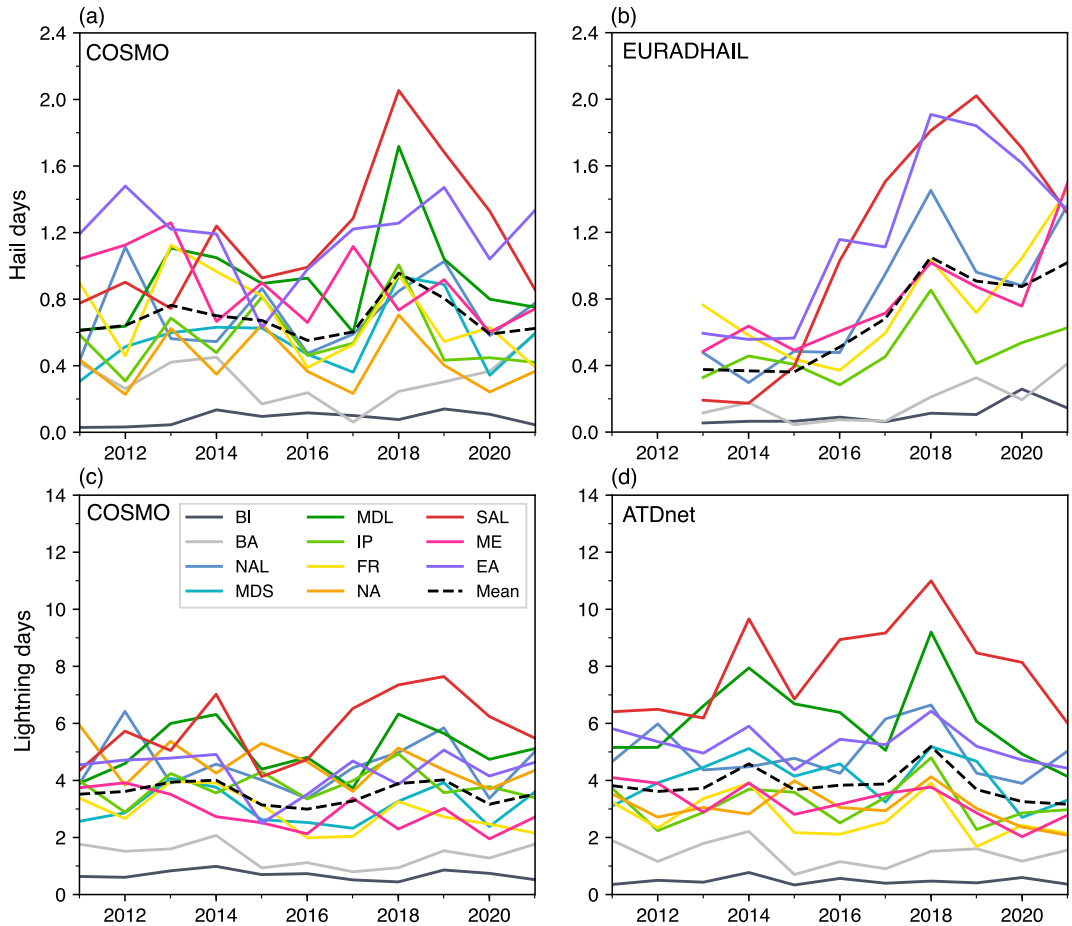

Figure 8. Interannual variations in hail (a, b) and lightning (c, d) days in different subdomains from (a, c) COSMO, (b) EURADHAIL, and (d) ATDnet. No EURADHAIL data is shown for MDS, MDL, and NA due to low data coverage. All subdomains, except MDS, focus exclusively on land.

4.4. Seasonal and Diurnal Cycles

The seasonal and diurnal cycles of hail occurrence over the European domain show comparatively minor spatial variations. For most subdomains, the hail peak occurs in summer, except for the MD and NA regions, which experience their peak in autumn (Figure 4b). Over land, the peak in hail generally aligns with the period of highest convective available potential energy (CAPE, see Figure S9 in Supporting Information S1) and heavy precipitation events (Figure 4a). This pattern is not observed in the southern Alpine domain (SAL) and the Iberian Peninsula (IP), where the peak in heavy precipitation occurs in autumn related to Mediterranean cyclones rather than during the peak hail season. In oceanic regions in the MDS subdomain, despite high CAPE values in summer, hail occurrence remains low until early autumn. This is because a vertical temperature inversion with high convective inhibition (CIN) over the ocean during summer inhibits convection initiation. The more frequent large-scale disturbances over the Mediterranean in autumn lead to a greater likelihood of hail cell development.

The seasonal cycles observed in the COSMO simulation largely agree with EURADHAIL in terms of peak season and magnitude (Figure 4d). The main discrepancy between the data sets is the later peak in FR and CE in COSMO compared to EURADHAIL. Because of missing data over the Mediterranean Sea, it remains difficult to evaluate the seasonal cycle in COSMO, which shows a peak in hail occurrence in September and October. ESWD reports along the western Italian coast indicate a later peak month than reports over land (Figure 9c), which is in line with the COSMO peak month over the Mediterranean Sea.

The diurnal cycles of hail occurrence are similar in the subdomains where the hail frequency peaks in the same season. For instance, continental subdomains, which show peak hail occurrence during summer, have a diurnal

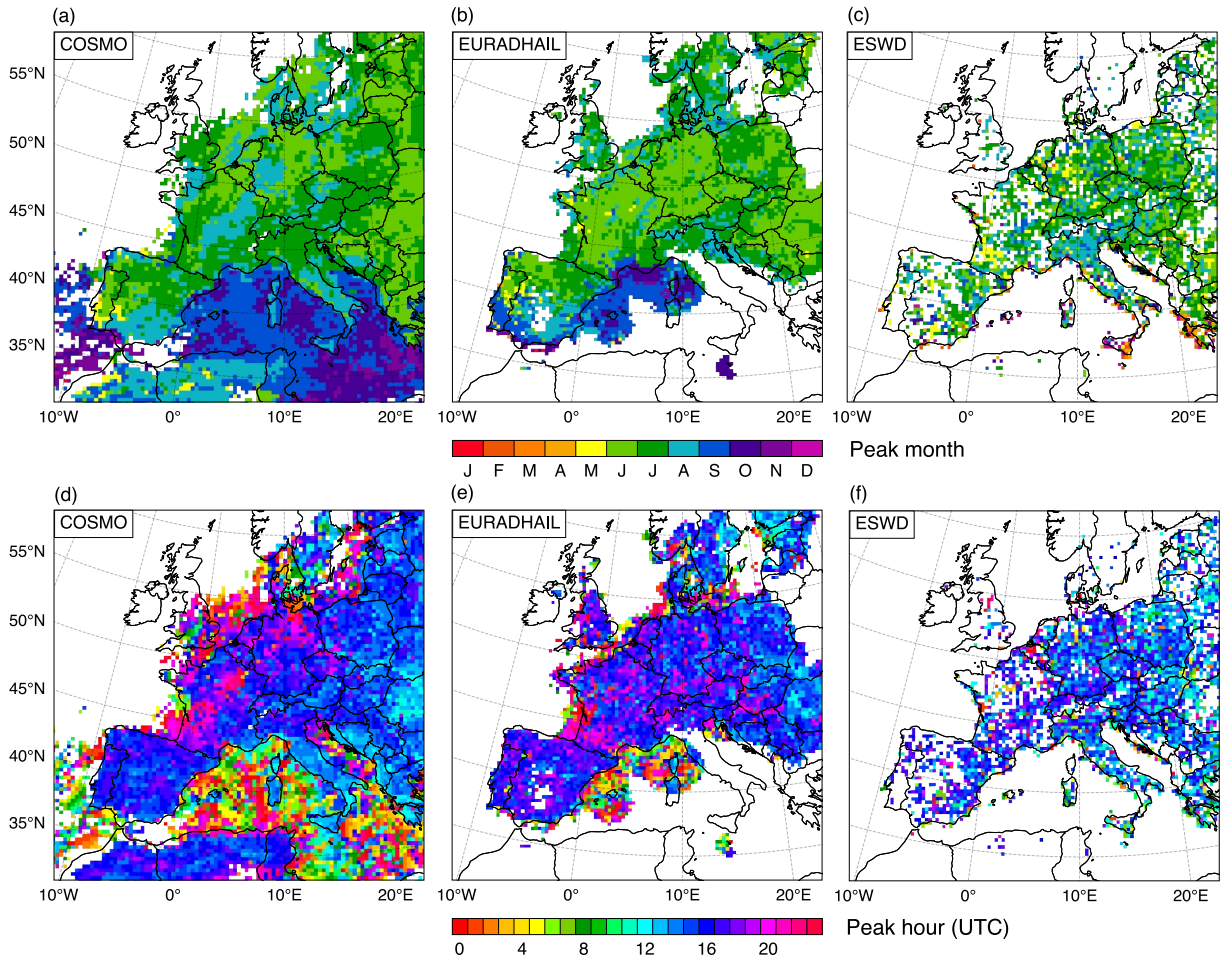

Figure 9. (a–c) Peak month of hail frequency and (d–f) peak hour (UTC) of hail frequency from (a, d) COSMO HAILCAST (2011–2021), (b, e) EURADHAIL (2013–2021), and (c, f) ESWD (2011–2021) from January to December. Hail frequency is aggregated to 30 km grid spacing to determine the peak occurrence.

cycle that peaks in the late afternoon at a similar local time. The earliest peak in the diurnal cycle occurs in EA around 13 UTC, whereas the latest peak is observed in FR around 16 UTC (Figure 9d). A distinct diurnal cycle is seen over the Mediterranean Sea, where hail events mainly occur in autumn. These events typically begin in the late evening and peak in the early morning, as daytime temperature inversions over the ocean inhibit convection during peak solar insulation.

Compared to observations, COSMO simulates similar diurnal cycles, with a close agreement in peak hours (Figure 9) and, to a lower degree, in peak frequency (Figure 5). All three data sets show a similar east-to-west increase in peak hour, whereas EURADHAIL tends to display later peak hours in the eastern part of the domain than the other data sets. This east-to-west shift of the diurnal hail peak is consistent with the differences between local time and UTC.

4.5. Hail Size Categories and Frequency Distributions

The COSMO validation so far demonstrated that the simulation accurately captures the geographical patterns, and the seasonal and diurnal cycles of hail occurrence across Europe. However, until now, we have not taken full advantage of the hail diameter output offered by the HAILCAST in COSMO, as our analysis has jointly considered all hail occurrences with a maximum hail diameter above 12.5 mm.

The limited availability of hail size observations poses a challenge for validating the hail size from COSMO. A comparison between different available data sets and the gridpoint-based COSMO daily maximum hail size frequency distribution is shown in Figure 10a. Compared to ESWD, the COSMO HAILCAST hail size

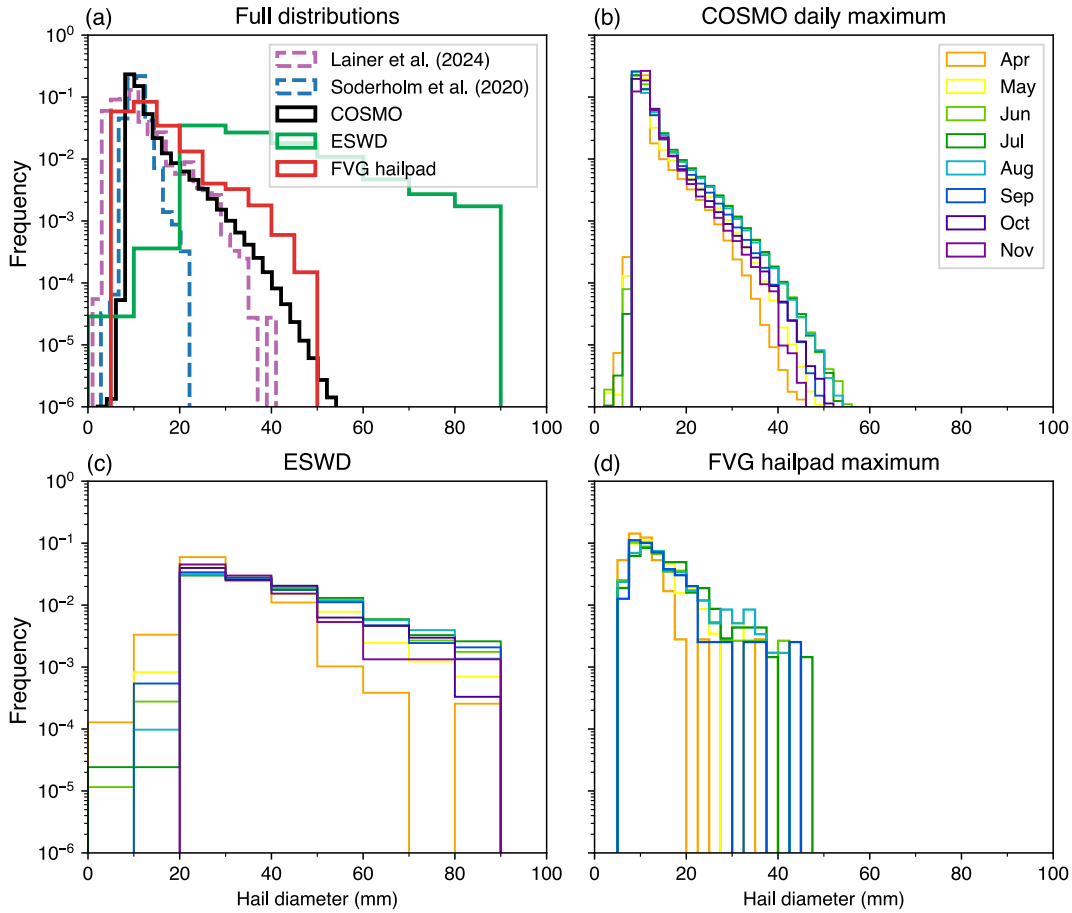

Figure 10. Normalized frequency of (a) full hail diameter distributions of COSMO daily maximum per gridpoint (2011–2021, black line), ESWD crowd-sourced reports (2011–2021, green line), daily maximum hail diameter across all FVG hail pads (1988–2016, red line) and single event drone-based hail diameter observations from Argentina (Soderholm, 2019, blue line) and Switzerland (Lainer et al., 2024, magenta line). For the COSMO, ESWD, and FVG hail pad data sets, the monthly distributions (April to November) are shown in (b–d). Dashed lines represent distributions from individual events, and solid bars indicate distributions based on multiyear observations.

distribution does not represent the distribution's tail of very large hail sizes correctly. The maximum simulated hail size is 75.5 mm. In contrast, ESWD reports a maximum hail size of 150 mm. This discrepancy is likely due to the inadequate simulation of large hailstones exceeding 40 mm in diameter by HAILCAST. One possible reason for this limitation is a too short simulated hail growth cycle, as the HAILCAST diagnostic does not consider the horizontal motion of hailstone in 3D flows. Further, HAILCAST is run every 5 min in our simulation, potentially missing strong updraft within the 5 min time windows. To reduce computing time, a compromise of 5 min HAILCAST runs was chosen for this study. For shorter simulations, a shorter time step might improve the COSMO hail size distribution. Nonetheless, case studies of hail events over the Adriatic Sea with the Weather Research and Forecasting (WRF) model including HAILCAST at every time step do not show pronounced increases in hailstone size (Malečić et al., 2022) compared to simulations with a HAILCAST time step of 5 min (Malečić et al., 2023). Additionally, crowd-sourced reports predominantly featuring large hailstones might misrepresent hail size distributions, leading to an overemphasis on the occurrence of larger hailstones. This bias is intensified by the limited observations of hailstones smaller than 20 mm, and a lack of small hail days in the ESWD data set, while such occurrences are part of the COSMO data set. Crowdsourcing applications with an automated reporting functionality capture a comparatively much larger number of small hail than the ESWD data set (compare Barras et al., 2019).

Close agreement is seen between COSMO and the FVG hail pad observations in northeastern Italy for hail diameters between 10 and 30 mm. The hail pads report relatively more hailstones with a diameter between 30 and

40 mm than COSMO, but no hailstones above 45 mm. Because of their relatively small impact area, hail pads underestimate the occurrence of large hailstones, as can be seen when compared to the ESWD distribution.

Drone-based measurements from a single hail event by Lainer (2024) revealed a distribution similar to the climatological COSMO distribution, whereas a drone survey conducted in Argentina (Soderholm, 2019) shows generally smaller hailstone than the COSMO distribution. However, a single observed event is clearly insufficient to validate a climatological data set, and a good agreement might have occurred by chance. Although drone-based observations offer direct size estimation and a higher probability of capturing the largest hailstones compared to other ground-based hail sensors, this approach's operational application and evaluation over extended domains remain challenging. This is mainly due to its limited spatial coverage, dependence on daylight, and the need for prior knowledge of hail events. Furthermore, if the drone survey is delayed, the hailstones start melting, leading to an underestimation of the hail size. To further assess model performance, more comprehensive measurements of hail size distributions across multiple events are needed.

A comparison of hail diameter distributions across various months, as illustrated in Figures 10b–10d, reveals that hailstorms in April produce fewer very large hailstones compared to other months. This is due to the lower CAPE. During the summer months, the size distribution of hailstones shifts toward larger sizes, reflecting higher energy availability. Finally, in autumn, the hail size distributions shift again to smaller hailstones. Compared to ESWD reports and FVG hailpad observations, COSMO HAILCAST successfully captures these seasonal variations in hailstone size.

The comparison of hail size distributions from modeling and observations shows large differences between the data sets. With the current analysis, we cannot say to which extent these differences are a result of model deficiencies, biases in the observations or differences in data set properties such as temporal and spatial resolution. Further model sensitivity studies and hail observations are needed to address these questions. In the subsequent analysis, we use the COSMO hail size outputs to describe differences between hail days of varying severity. However, this comparison is qualitative, given the uncertainties associated with COSMO hail diameters.

The main hotspots for severe hail days (defined as hail days with a maximum hail diameter larger than 20 mm) are the Po Valley region, northeastern Spain and southern Italy (Figure 11). These areas generally align with hail proxies for severe hail events, which also indicate a high occurrence in southern Europe (Hand & Cappelluti, 2011; Kahraman et al., 2024). The COSMO climatology, derived from HAILCAST outputs of explicitly simulated hail occurrence, shows more distinct hotspots for severe hail days than hail proxies, which depict more widespread areas of severe hail occurrence (Hand & Cappelluti, 2011; Kahraman et al., 2024). It is worth noting that the main hotspots for large hail, based on ESWD reports, are located over eastern Austria and Germany, whereas the Po Valley hotspot is less prominent (Taszarek et al., 2020). Although COSMO may miss some large hail events in the eastern Alps, the ESWD-based climatology might underestimate hail occurrence in the Po Valley relative to Eastern Europe, possibly due to a higher reporting activity in the latter region.

4.6. Comparison With Existing European Hail Climatologies

The COSMO climatology reveals similar hail hotspots across Europe as found in previous observational and model-based studies. Key regions of frequent hail occurrence, such as the Po Valley, the Carpathian basin, and the Pyrenees in summer, as well as the Mediterranean Sea in autumn, have also been highlighted in studies based on hail proxies (Hand & Cappelluti, 2011; Kahraman et al., 2024; Mohr et al., 2015; Prein & Holland, 2018; Punge et al., 2014) and, at lower spatial resolution, in global satellite-based products (Bang & Cecil, 2019; Cecil & Blankenship, 2012; Ferraro et al., 2015; Mroz et al., 2017). Hotspots along the Pyrenees, east of the Massif Central in France and along the northern pre-Alps have also been identified with a radar-based product (Fluck et al., 2021). The hail days around Italy in COSMO show a similar distribution as a multi-year analysis of proxy-based hail days using overshooting cloud tops combined with crowd-sourced hail observations and regional reanalysis data (Giordani et al., 2024), with peaks occurring over land in summer and over the ocean in autumn.

One key difference from previous model-based climatologies that rely on hail proxies is the relative intensity of hail hotspots over Europe. For instance, Kahraman et al. (2024) identified the highest severe hail potential during autumn over the Mediterranean Sea and Greece. Similarly, Prein and Holland (2018) and Hand and Cappelluti (2011) showed the highest annual numbers of hail days and events, respectively, over the Mediterranean Sea or coastal areas. Mohr et al. (2015), however, presented an annual distribution of hail potential that aligns more

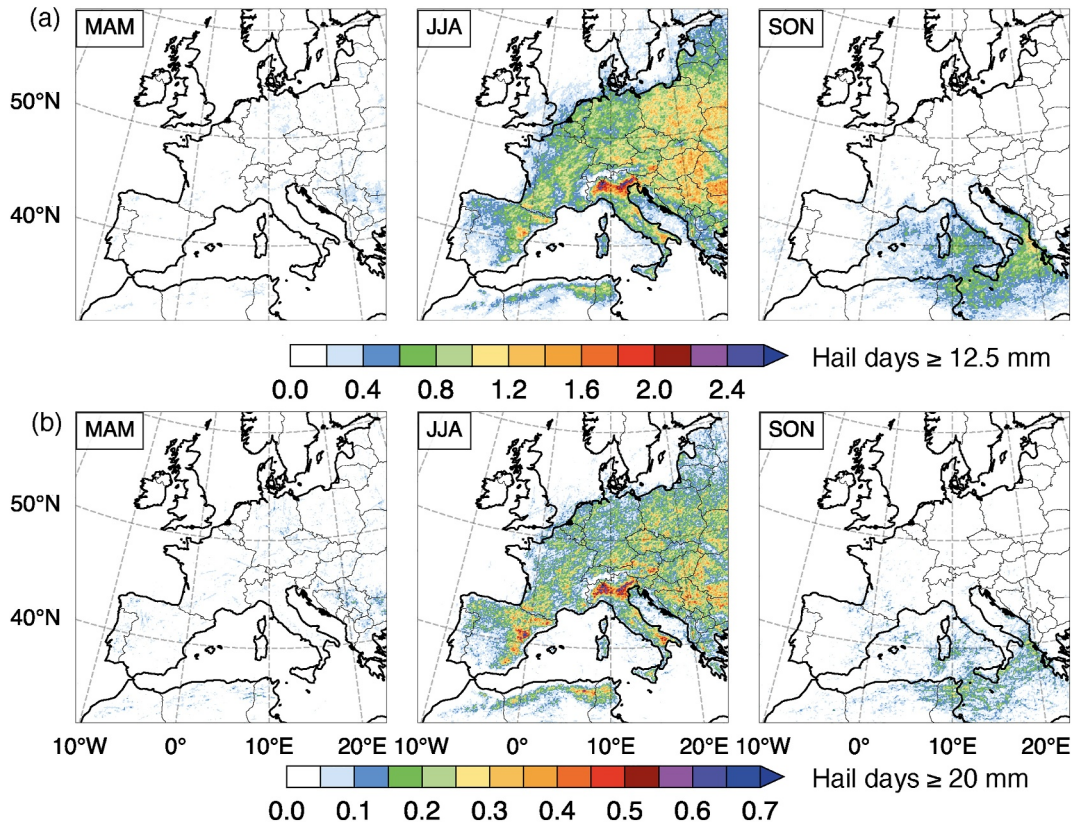

Figure 11. Seasonal-mean hail days from COSMO HAILCAST with (a) maximum hail diameter ≥12.5 mm and (b) ≥20 mm in MAM, JJA, and SON during 2011–2021. All data are shown with 1.5σ Gaussian smoothing applied spatially.

closely with the findings of this study, particularly highlighting the Po Valley region, the northern pre-Alps, and the Carpathian basin as significant hail frequency hotspots.

5. European Lightning Climatology

5.1. Lighting Stroke Density and Lightning Days

In addition to hail, the LPI was also calculated online in the COSMO simulation, enabling the analysis of lightning activity across Europe. The LPI was calibrated using ATDnet observations (see Section 2.7) to estimate lightning stroke density and lightning days (Figure 12). A comparison of the seasonal and diurnal lightning climatology between COSMO and ATDnet is presented below.

Compared to ATDnet observations, the COSMO simulation captures a similar spatial distribution of lightning strokes across Europe, with summer hotspots along the slopes of mountain ranges such as the Alps, Pyrenees, and the Carpathians (Figure 12). Additional summer hotspots occur in the Ebro Valley in eastern Spain and over the Atlas Mountains in northwestern Africa. The main lightning activity over the Mediterranean Sea occurs in autumn. In Northern Europe, COSMO simulates a higher lightning stroke density than ATDnet, although both show a similar number of lightning days. Overall, the spatial agreement between COSMO and ATDnet is slightly better for lightning days than for stroke density, indicating that while the model accurately represents periods with elevated lightning potential, the LPI cannot fully estimate the precise number of strokes. Further, it has to be noted that, based on the LPI calibration method, the absolute number of lightning strokes in the COSMO climatology depends directly on the number of lightning strokes in the ATDnet data set. Any undercatchment of lightning by the ATDnet network will also be reflected in the COSMO output.

Several differences between the data sets are noticeable. In the COSMO simulation, lightning hotspots tend to be more widespread and peak at lower values than the ATDnet observations, likely due to differences in spatial resolution. Similar shortcomings have been noticed for hail hotspots, where the COSMO model does not

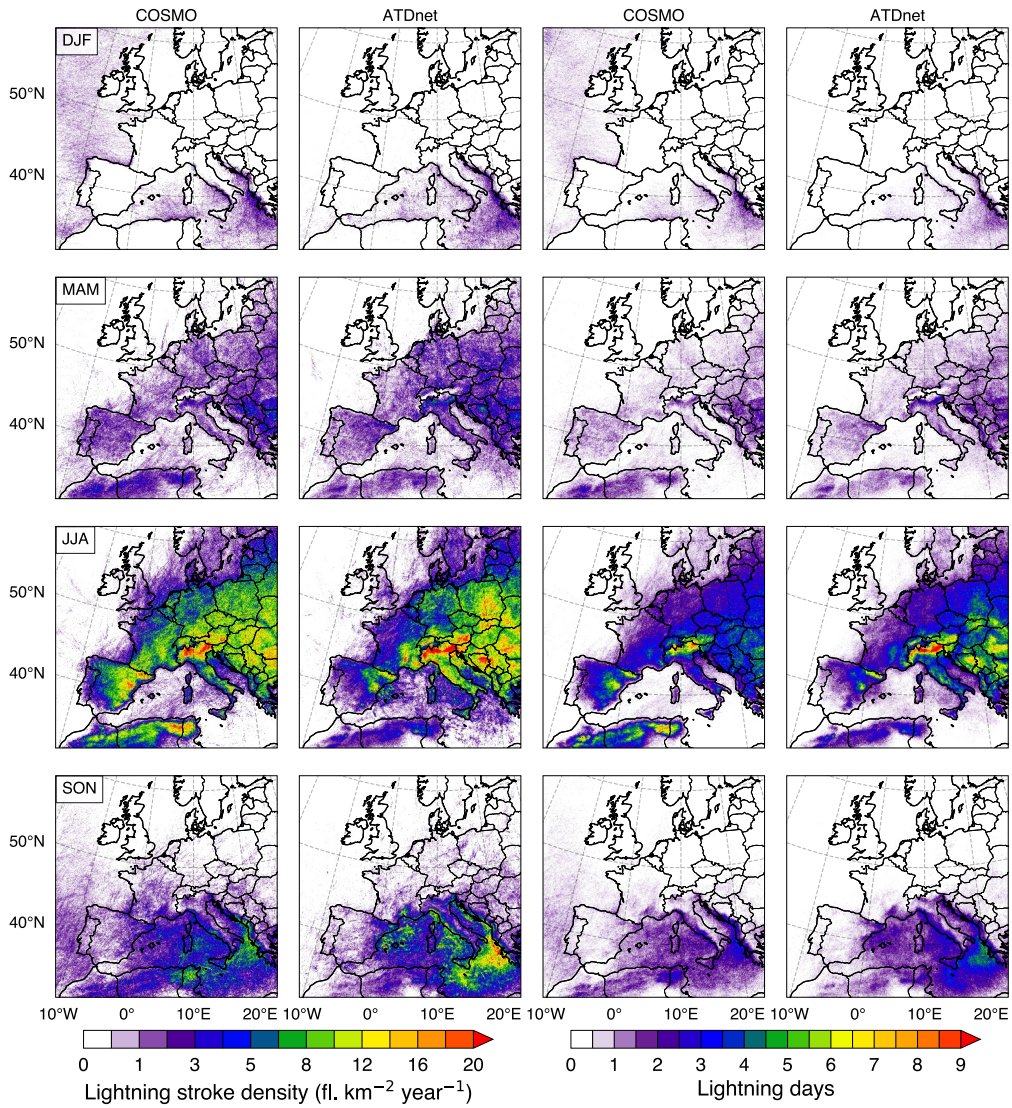

Figure 12. Spatial distribution of lightning stroke density (first two columns) and lightning days (third and fourth columns) from COSMO and ATDnet for different seasons (DJF to SON, top to bottom rows) during 2011–2021. All data are presented at a spatial resolution of 2.2 km.

accurately represent hail hotspots along the northern Swiss pre-Alps (Figure 7). Additionally, COSMO struggles to capture detailed lightning hotspots over the Carpathian Mountains and Balkan regions. The lightning activity along the Atlas Mountains, observed in COSMO, is absent in the ATDnet data set, most likely because North Africa falls outside ATDnet's high-accuracy detection range (Enno et al., 2016).

The interannual variability in COSMO and ATDnet agrees well (Pearson's correlation coefficient above 0.5 for most subdomains) with periods of enhanced lightning activity around 2014 and 2018 (Figure 8), which aligns with findings from previous studies (Manzato, Serafin, et al., 2022; Poelman et al., 2016). Main differences can be seen for north Africa and the British Isles, where LPI tends to overestimate the lightning day frequency as also seen in the spatial patterns in Figure 12. Further, eastern Europe shows a similar number of annual lightning days in COSMO and ATDnet with small interannual variations (Pearson's correlation coefficient of 0.27).

The seasonal cycles of lightning activity in COSMO align well with ATDnet, showing a peak between June and August over continental regions (Figure 4, see also Figure S11 in Supporting Information S1), and in September and October over the Mediterranean Sea. However, the diurnal cycles in COSMO peak 1–2 hr too early, with peaks between 14 and 16 UTC, compared to ATDnet's peaks between 15 and 17 UTC (Figure 5, see also Figure

S11 in Supporting Information S1). Notably, this difference in diurnal cycles has not been observed when comparing hail in COSMO and ESWD reports. The most significant difference in diurnal cycles between the model and observations occurs over the Mediterranean Sea. In this region, ATDnet shows a distinct peak around 08 UTC, whereas COSMO displays a weaker diurnal cycle, with a peak in the early morning. The model also indicates a stronger influence of continental convection over the Adriatic Sea, with a peak in the late evening (Figure S5 in Supporting Information S1). This discrepancy may be related to the model's horizontal resolution, which may not accurately capture convection initiation over the Adriatic. Similar limitations were noted in an earlier study, where COSMO struggled to simulate early morning hail events along the Croatian coast (Cui et al., 2023).

The simulated spatial patterns, as well as the seasonal and diurnal cycles of lightning occurrence, are qualitatively similar to those of hail, reflecting the distribution and frequency of convective systems in the model. The main difference appears around the Carpathian Mountains, where the hail day climatology shows more pronounced hotspots compared to lightning. Additionally, there is significantly more lightning than hail activity over the Mediterranean Sea in autumn, especially in the Adriatic Sea west of Greece. This suggests that COSMO successfully initiates convection in this region, however more often, leading to lightning instead of producing hail.

5.2. Comparison With Existing European Lightning Climatologies

In contrast to hail, numerous European lightning climatologies are already available, and COSMO shows close agreement with these in terms of the spatial distribution and seasonal cycle of lightning activity (e.g., Anderson & Klugmann, 2014; Galanaki et al., 2018; Kahraman et al., 2022; Kolendowicz et al., 2017; Manzato, Serafin, et al., 2022; Petracca et al., 2024; Taszarek et al., 2019; Wapler, 2013). Our estimate of lightning days falls at the lower boundary of the observed range, similar to Wapler (2013), who reported up to 7 lightning days per year in southern Germany. Many studies, however, show lightning day peaks of up to 30 days per year, which exceeds the maximum of 20 days along the southern Alpine slopes in our study. Since the LPI must be calibrated to represent lightning strokes and days, these values strongly depend on the observational data set used for calibration. ATDnet, for example, is known to represent cloud-to-ground flashes by about 89% and in-cloud flashes by 24% (Enno et al., 2016), which can partly explain the relatively low numbers of lightning days derived from the LPI.

A key difference between the model and observations, as noted in the comparison with ATDnet, is seen in the diurnal cycle, particularly over the Mediterranean Sea, where COSMO does not capture the early morning peak observed by ATDnet. However, Galanaki et al. (2018) and Petracca et al. (2024) presented a weaker diurnal cycle for the Mediterranean Sea, which aligns more closely with the COSMO simulation. Additionally, the high lightning activity along the Atlas Mountains is consistent with the findings of Galanaki et al. (2018), based on the ZEUS lightning detection system, indicating that the LPI can represent lightning even in desert regions.

Overall, the lightning climatology derived from the LPI shows good qualitative agreement with observations, demonstrating the value of this online lightning diagnostic in kilometer-scale climate simulations. To further explore the performance of LPI and how it translates into lightning strokes, calibration with other lightning data sets is needed in future studies.

6. Conclusions and Outlook

We presented an 11-year European hail and lightning climatology based on a convection-permitting climate simulation that was run with online hail and lightning diagnostics. Additionally, we introduced EURADHAIL, a new European-wide high-resolution hail proxy, based on the 2D OPERA radar composite and ATDnet lightning strokes. The COSMO model-based hail climatology aligns qualitatively well with observational data sets, such as EURADHAIL and ESWD crowd-sourced reports, in terms of spatial distribution, seasonal cycle (peak month), and diurnal cycle (peak hour) of hail occurrence. The simulation identified the highest hail occurrence frequencies along the northern and southern pre-Alps, the Pyrenees, the Carpathian Mountains, and over the Mediterranean Sea, consistent with findings from previous model-based (Hand & Cappelluti, 2011; Kahraman et al., 2024; Mohr et al., 2015; Prein & Holland, 2018; Punge et al., 2014) and satellite-based hail climatologies (Bang & Cecil, 2019; Cecil & Blankenship, 2012; Ferraro et al., 2015; Mroz et al., 2017).

Because of the good representation of the diurnal cycle of convection in COSMO, we were able to analyze the diurnal cycles of hail occurrence across Europe. Most regions exhibit a peak hail activity between 12 and 18 UTC.

The main exception is the Mediterranean Sea, where the diurnal cycle of hail occurrence shows a weak peak around 04 UTC. Although the COSMO simulation qualitatively captures the diurnal cycle across most of the model domain, it underestimates early morning convective activity in the Adriatic Sea, a pattern also observed by Cui et al. (2023).

A unique feature of the COSMO HAILCAST output is its ability to provide information on hail size, which can be aggregated over the 11-year simulation to obtain local hail size distributions. It appears that the model tends to underestimate the frequency of large hailstones (>30 mm) compared to ESWD reports. Moreover, compared to hail pad observations, the modeled distribution shows similar hail sizes. Validating hail size distributions remains difficult due to the limited availability of observational data and differences in data set properties such as temporal and spatial resolution.

The COSMO lightning climatology shows a qualitatively good spatial and seasonal representation of lightning occurrence across continental Europe compared to observations (e.g., Anderson & Klugmann, 2014; Kahraman et al., 2022; Taszarek et al., 2019; Wapler, 2013). COSMO simulates an earlier peak in the diurnal lightning cycle over the continent, and generally shows lower lightning activity over the ocean than ATDnet. Overall, lightning and hail hotspots over Europe coincide in location and time as both hazards are caused by severe convective storms.

There is a growing need for reliable observations, particularly when considering extreme events such as hail and lightning. In this paper, we introduced EURADHAIL, a new valuable hail proxy for the purpose of model evaluation, with the potential for further development. By incorporating volumetric reflectivity and freezing level height data, EURADHAIL could improve its ability to estimate hail size and remove spurious clutters. Moreover, calibration using available hail sensors and quality-checked hail reports could enhance the regional applicability and accuracy of the data set. Such advancements in observational data sets can benefit future research, ultimately contributing to refinements in hail modeling in weather and climate models.

Building on the qualitative good performance of the COSMO simulation with respect to the continental seasonal and diurnal cycle demonstrated in this study, high-resolution simulations provide an opportunity for diverse future research projects on severe convective storms and their impacts. For example, the high temporal resolution of the hail output, available at 5-min intervals, enables detailed investigations into the drivers of hail production and the evolution of hail cells. Additionally, the consistent, European-wide hail data set provides a larger study domain compared to previous data sets, facilitating analysis of hail impact on infrastructure and agriculture across different climatic zones of Europe (Portmann et al., 2024; Schmid et al., 2024). The high-resolution output variables also allow for broader applications, including studies on the societal impacts of severe weather events, such as strong winds, heavy precipitation, dry spells, and winter storms. Furthermore, our findings show that COSMO accurately simulates the present-day climatology of convective storms, suggesting strong potential for using the same methods in future climate simulations to assess the impact of climate change on hail and lightning. In a subsequent study, we will present results from pseudo-global warming simulations using the same COSMO model setup, to quantify the impacts of climate change on the occurrence of hail across Europe.

Appendix A: HAILCAST Artifact Filtering Algorithm

Under very specific and rare circumstances, HAILCAST can produce a hail signal that is not plausible, hereafter referred to as artifacts. These artifacts are usually co-located with steep orography and strong horizontal wind. In such situations, HAILCAST can be triggered by the locally strong vertical wind component that results from the horizontal wind impinging on the topography. The bulk of these artifacts occurs in the cold season, when there is supercooled water near the ground. As an effort to mitigate the effects of these rare HAILCAST artifacts, we developed an algorithm to filter them out. This algorithm eliminates hail values from HAILCAST that exist in the absence of rain rates exceeding 4 mm hr^{-1}. The algorithm allows for some temporal (±20 min) and spatial ($r = 17$ km) ambiguity in the co-location of hail and rain, taking into account possible advection of the rain. To this end, at each 5 min time step the maximum rain rate within a window of 45 min centered on the current time step is taken. The time-centered rain rate is thresholded by 4 mm hr^{-1}, yielding a binary mask. A binary dilation is applied through a circular disk kernel with a radius of 17 km to expand the binary mask. The resulting binary mask is applied to the raw HAILCAST field to yield the filtered HAILCAST field. The filtering algorithm is available through the following repository: https://doi.org/10.5281/zenodo.12799528 (Brennan, 2024). A similar approach

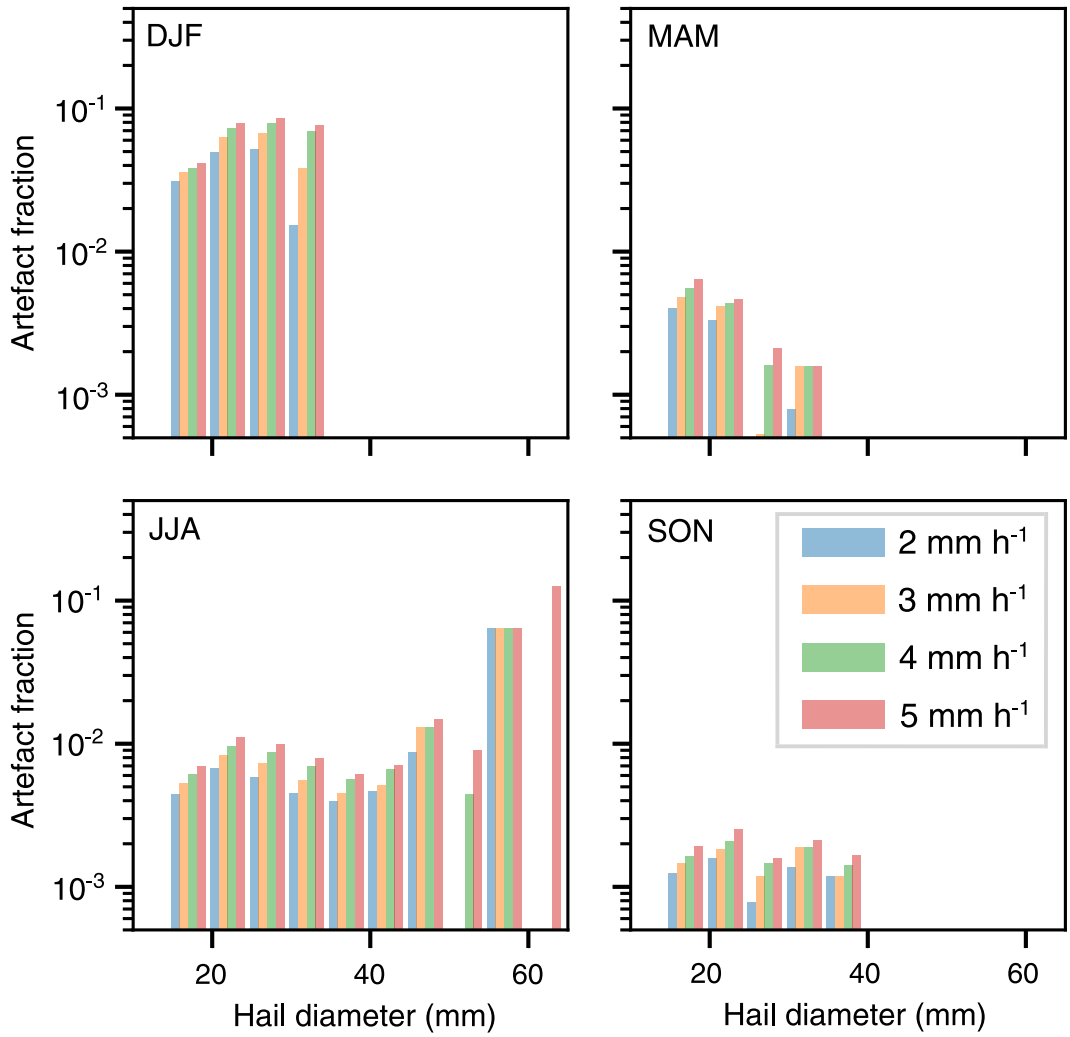

Figure A1. Histogram of the fraction of total HAILCAST grid-points per 5 mm bin that are classified as artifacts by the filtering algorithm (Section Appendix A) for different rain rate thresholds. These sensitivity tests were done with the COSMO output in the year 2021.

was applied by Sanderson et al. (2015), who pre-filtered their data based on the precipitation amount before conducting calculations in their hail model.

To investigate the filtering algorithm's sensitivity to the rain rate threshold, the filter was applied to a subset of the simulation (1 year) with rain rate thresholds of 2, 3, 4, and 5 mm hr^{-1}. The response of the filtering algorithm to the different thresholds was found to be linear and robust. Eventually, a threshold of 4 mm hr^{-1} was chosen to be applied to the entire simulation, as in some hail size bins and seasons (e.g., 30–35 mm in DJF and 50–55 mm in JJA) a reduced change in the filtering response was found for precipitation thresholds ≥4 mm hr^{-1} (Figure A1). As expected, the highest artifact fraction is found in DJF (4%–7%, depending on hail size), whereas for all but the largest diameters in JJA, artifacts account for less than 1% of the hail grid-points.

Data Availability Statement

IMERG precipitation product (Huffman et al., 2023) can be retrieved from https://gpm.nasa.gov/data/directory, E-OBS gridded data set (Cornes et al., 2018) from https://www.ecad.eu/download/ensembles/download.php, EURADCLIM (Overeem et al., 2023) from https://dataplatform.knmi.nl/dataset/rad-opera-hourly-rainfall-accumulation-euradclim-2-0. ESWD crowd-sourced reports (Dotzek et al., 2009) are provided through the European Weather Observer via https://www.eswd.eu/. EURADHAIL radar-derived hail data set (Cui &

Thurnherr, 2024) is accessible via https://doi.org/10.3929/ethz-b-000701924, FVG hailpad data set (Manzato, Cicogna, et al., 2022) is available at https://www.meteo.fvg.it/grandine.php. Due to the large size, a selection of the COSMO model output (Thurnherr & Cui, 2024) is available via https://doi.org/10.3929/ethz-b-000701925.

Acknowledgments
This study was funded by the Swiss National Science Foundation (SNSF) Sinergia Grant CRSII5_201792 (scClim project). The simulations were supported by a grant from the Swiss National Supercomputing Center (CSCS). We thank the Center for Climate Systems Modeling (C2SM), particularly Ruth Lorenz for the technical support. Further, we thank our colleagues on the scClim project for fruitful exchange during project meetings. We further thank MeteoSwiss for the access to observational data (POH, APGD, CombiPrecip, and IDAWEB) and Christian Zeman for his help with the Swiss station-based precipitation observations (IDAWEB). The authors acknowledge NASA for the IMERG data, EU-FP6 project UERRA, Copernicus Climate Change Service, and the data providers in the ECA&D project for the E-OBS data, EUMETNET for the OPERA data, KNMI for the EURADCLIM data, the UK Met Office for ATDnet data, ESSL for the ESWD data, and ARPA FVG-OSMER for the hailpad data. We extend our gratitude to the volunteers and observers for their contributions in maintaining the hail observations. We appreciate the constructive feedback from three anonymous reviewers. Open access publishing facilitated by Eidgenossische Technische Hochschule Zurich, as part of the Wiley - Eidgenossische Technische Hochschule Zurich agreement via the Consortium Of Swiss Academic Libraries.

References

Adams-Selin, R. D., Clark, A. J., Melick, C. J., Dembek, S. R., Jirak, I. L., & Ziegler, C. L. (2019). Evolution of WRF-HAILCAST during the 2014–16 NOAA/hazardous weather testbed spring forecasting experiments. *Weather and Forecasting*, *34*(1), 61–79. https://doi.org/10.1175/WAF-D-18-0024.1

Adams-Selin, R. D., & Ziegler, C. L. (2016). Forecasting hail using a one-dimensional hail growth model within WRF. *Monthly Weather Review*, *144*(12), 4919–4939. https://doi.org/10.1175/mwr-d-16-0027.1

Afanasyev, A., Bianco, M., Mosimann, L., Osuna, C., Thaler, F., Vogt, H., et al. (2021). GridTools: A framework for portable weather and climate applications. *SoftwareX*, *15*, 100707. https://doi.org/10.1016/j.softx.2021.100707

Anderson, G., & Klugmann, D. (2014). A European lightning density analysis using 5 years of ATDnet data. *Natural Hazards and Earth System Sciences*, *14*(4), 815–829. https://doi.org/10.5194/nhess-14-815-2014

ARPA FVG–OSMER. (2021). Presentation of the aggregate database of panels hit by hail in the plain of Friuli Venezia Giulia during the period April–September 1988–2016 [Dataset]. Retrieved from https://www.meteo.fvg.it/grandine.php

Baldauf, M., Seifert, A., Förstner, J., Majewski, D., Raschendorfer, M., & Reinhardt, T. (2011). Operational convective-scale numerical weather prediction with the COSMO Model: Description and sensitivities. *Monthly Weather Review*, *139*(12), 3887–3905. https://doi.org/10.1175/MWR-D-10-05013.1

Ban, N., Caillaud, C., Coppola, E., Pichelli, E., Sobolowski, S., Adinolfi, M., et al. (2021). The first multi-model ensemble of regional climate simulations at kilometer-scale resolution, part I: Evaluation of precipitation. *Climate Dynamics*, *57*(1–2), 275–302. https://doi.org/10.1007/s00382-021-05708-w

Ban, N., Schmidli, J., & Schär, C. (2014). Evaluation of the convection-resolving regional climate modeling approach in decade-long simulations. *Journal of Geophysical Research: Atmospheres*, *119*(13), 7889–7907. https://doi.org/10.1002/2014JD021478

Ban, N., Schmidli, J., & Schär, C. (2015). Heavy precipitation in a changing climate: Does short-term summer precipitation increase faster? *Geophysical Research Letters*, *42*(4), 1165–1172. https://doi.org/10.1002/2014gl062588

Bang, S. D., & Cecil, D. J. (2019). Constructing a multifrequency passive microwave hail retrieval and climatology in the GPM domain. *Journal of Applied Meteorology and Climatology*, *58*(9), 1889–1904. https://doi.org/10.1175/JAMC-D-19-0042.1

Barras, H., Hering, A., Martynov, A., Noti, P.-A., Germann, U., & Martius, O. (2019). Experiences with >50, 000 crowdsourced hail reports in Switzerland. *Bulletin of the American Meteorological Society*, *100*(8), 1429–1440. https://doi.org/10.1175/bams-d-18-0090.1

Belušić, A., Prtenjak, M. T., Güttler, I., Ban, N., Leutwyler, D., & Schär, C. (2018). Near-surface wind variability over the broader Adriatic region: Insights from an ensemble of regional climate models. *Climate Dynamics*, *50*(11–12), 4455–4480. https://doi.org/10.1007/s00382-017-3885-5

Bennett, A. J., Gaffard, C., Nash, J., Callaghan, G., & Atkinson, N. C. (2011). The effect of modal interference on VLF long-range lightning location networks using the waveform correlation technique. *Journal of Atmospheric and Oceanic Technology*, *28*(8), 993–1006. https://doi.org/10.1175/2011JTECHA1527.1

Betz, H. D., Schmidt, K., Laroche, P., Blanchet, P., Oettinger, W. P., Defer, E., et al. (2009). LINET—An international lightning detection network in Europe. *Atmospheric Research*, *91*(2–4), 564–573. https://doi.org/10.1016/j.atmosres.2008.06.012

Blašković, L., Jelić, D., Malečić, B., Omazić, B., Güttler, I., & Telišman Prtenjak, M. (2023). Trend analysis and climatology of hail in Croatia. *Atmospheric Research*, *294*, 106927. https://doi.org/10.1016/j.atmosres.2023.106927

Brennan, K. P. (2024). Hailcast filter as used for climate simulations [Software]. *Zenodo*. https://doi.org/10.5281/zenodo.12799527

Brennan, K. P., Sprenger, M., Walser, A., Arpagaus, M., & Wernli, H. (2024). An object-based and Lagrangian view on an intense hailstorm day in Switzerland as represented in COSMO-1E ensemble hindcast simulations. *EGUsphere*, *2024*, 1–31. https://doi.org/10.5194/egusphere-2024-2148

Bright, D. R., Jewell, R. E., Wandishin, M. S., & Weiss, S. J. (2005). A physically-based parameter for lightning prediction and its calibration in ensemble forecasts. *85th AMS Annual Meeting*.

Brimelow, J. C., Reuter, G. W., & Poolman, E. R. (2002). Modeling maximum hail size in Alberta thunderstorms. *Weather and Forecasting*, *17*(5), 1048–1062. https://doi.org/10.1175/1520-0434(2002)017⟨1048:MMHSIA⟩2.0.CO;2

Brisson, E., Blahak, U., Lucas-Picher, P., Purr, C., & Ahrens, B. (2021). Contrasting lightning projection using the lightning potential index adapted in a convection-permitting regional climate model. *Climate Dynamics*, *57*(7–8), 2037–2051. https://doi.org/10.1007/s00382-021-05791-z

Brogli, R., Heim, C., Mensch, J., Sørland, S. L., & Schär, C. (2023). The pseudo-global-warming (PGW) approach: Methodology, software package PGW4ERA5 v1.1, validation, and sensitivity analyses. *Geoscientific Model Development*, *16*(3), 907–926. https://doi.org/10.5194/gmd-16-907-2023

Carver, A. R., Ross, J. D., Augustine, D. J., Skagen, S. K., Dwyer, A. M., Tomback, D. F., & Wunder, M. B. (2017). Weather radar data correlate to hail-induced mortality in grassland birds. *Remote Sensing in Ecology and Conservation*, *3*(2), 90–101. https://doi.org/10.1002/rse2.41

Cecil, D. J. (2009). Passive microwave brightness temperatures as proxies for hailstorms. *Journal of Applied Meteorology and Climatology*, *48*(6), 1281–1286. https://doi.org/10.1175/2009JAMC2125.1

Cecil, D. J., & Blankenship, C. B. (2012). Toward a global climatology of severe hailstorms as estimated by satellite passive microwave imagers. *Journal of Climate*, *25*(2), 687–703. https://doi.org/10.1175/JCLI-D-11-00130.1

Christensen, J. H., Carter, T. R., Rummukainen, M., & Amanatidis, G. (2007). Evaluating the performance and utility of regional climate models: The PRUDENCE project. *Climatic Change*, *81*(1), 1–6. https://doi.org/10.1007/s10584-006-9211-6

Cifelli, R., Doesken, N., Kennedy, P., Carey, L. D., Rutledge, S. A., Gimmestad, C., & Depue, T. (2005). The community collaborative rain, hail, and snow network: Informal education for scientists and citizens. *Bulletin of the American Meteorological Society*, *86*(8), 1069–1078. https://doi.org/10.1175/bams-86-8-1069

Coppola, E., Sobolowski, S., Pichelli, E., Raffaele, F., Ahrens, B., Anders, I., et al. (2018). A first-of-its-kind multi-model convection permitting ensemble for investigating convective phenomena over Europe and the Mediterranean. *Climate Dynamics*, *55*(1–2), 3–34. https://doi.org/10.1007/s00382-018-4521-8

Cornes, R. C., van der Schrier, G., van den Besselaar, E. J. M., & Jones, P. D. (2018). An ensemble version of the E-OBS temperature and precipitation data sets. *Journal of Geophysical Research: Atmospheres*, *123*(17), 9391–9409. https://doi.org/10.1029/2017jd028200

Cui, R., Ban, N., Demory, M.-E., Aellig, R., Fuhrer, O., Jucker, J., et al. (2023). Exploring hail and lightning diagnostics over the Alpine-Adriatic region in a km-scale climate model. *Weather and Climate Dynamics*, *4*(4), 905–926. https://doi.org/10.5194/wcd-4-905-2023

Cui, R., & Thurnherr, I. (2024). EURADHAIL: European-wide radar-based hail product from 2013-2021 [Dataset]. Retrieved from http://hdl.handle.net/20.500.11850/701924

Dessens, J. (1986). Hail in southwestern France. I: Hailfall characteristics and hailstrom environment. *Journal of Applied Meteorology and Climatology*, *25*(1), 35–47. https://doi.org/10.1175/1520-0450(1986)025⟨0035:HISFIH⟩2.0.CO;2

Doswell, C. A., Ramis, C., Romero, R., & Alonso, S. (1998). A diagnostic study of three heavy precipitation episodes in the western Mediterranean region. *Weather and Forecasting*, *13*(1), 102–124. https://doi.org/10.1175/1520-0434(1998)013⟨0102:ADSOTH⟩2.0.CO;2

Dotzek, N., Groenemeijer, P., Feuerstein, B., & Holzer, A. M. (2009). Overview of ESSL's severe convective storms research using the European severe weather database ESWD. *Atmospheric Research*, *93*(1–3), 575–586. https://doi.org/10.1016/j.atmosres.2008.10.020

Enno, S.-E., Anderson, G., & Sugier, J. (2016). ATDnet detection efficiency and cloud lightning detection characteristics from comparison with the HyLMA during HyMeX SOP1. *Journal of Atmospheric and Oceanic Technology*, *33*(9), 1899–1911. https://doi.org/10.1175/jtech-d-15-0256.1

Enno, S.-E., Sugier, J., Alber, R., & Seltzer, M. (2020). Lightning flash density in Europe based on 10 years of ATDnet data. *Atmospheric Research*, *235*, 104769. https://doi.org/10.1016/j.atmosres.2019.104769

Estermann, R., Rajczak, J., Velasquez, P., Lorenz, R., & Schär, C. (2025). Projections of heavy precipitation characteristics over the greater alpine region using a kilometer–scale climate model ensemble. *Journal of Geophysical Research: Atmospheres*, *130*(2), e2024JD040901. https://doi.org/10.1029/2024jd040901

Ferraro, R., Beauchamp, J., Cecil, D., & Heymsfield, G. (2015). A prototype hail detection algorithm and hail climatology developed with the advanced microwave sounding unit (AMSU). *Atmospheric Research*, *163*, 24–35. https://doi.org/10.1016/j.atmosres.2014.08.010

Ferro, C. A. T., & Stephenson, D. B. (2011). Extremal dependence indices: Improved verification measures for deterministic forecasts of rare binary events. *Weather and Forecasting*, *26*(5), 699–713. https://doi.org/10.1175/waf-d-10-05030.1

Fluck, E., Kunz, M., Geissbuehler, P., & Ritz, S. P. (2021). Radar-based assessment of hail frequency in Europe. *Natural Hazards and Earth System Sciences*, *21*(2), 683–701. https://doi.org/10.5194/nhess-21-683-2021

Fowler, H. J., Lenderink, G., Prein, A. F., Westra, S., Allan, R. P., Ban, N., et al. (2021). Anthropogenic intensification of short-duration rainfall extremes. *Nature Reviews Earth & Environment*, *2*(2), 107–122. https://doi.org/10.1038/s43017-020-00128-6

Gabella, M., & Notarpietro, R. (2002). Ground clutter characterization and elimination in mountainous terrain. Retrieved from https://www.copernicus.org/erad/online/erad-305.pdf

Galanaki, E., Lagouvardos, K., Kotroni, V., Flaounas, E., & Argiriou, A. (2018). Thunderstorm climatology in the Mediterranean using cloud-to-ground lightning observations. *Atmospheric Research*, *207*, 136–144. https://doi.org/10.1016/j.atmosres.2018.03.004

Galway, J. G. (1956). The lifted index as a predictor of latent instability. *Bulletin of the American Meteorological Society*, *37*(10), 528–529. https://doi.org/10.1175/1520-0477-37.10.528

Germann, U., Boscacci, M., Clementi, L., Gabella, M., Hering, A., Sartori, M., et al. (2022). Weather radar in complex orography. *Remote Sensing*, *14*(3), 503. https://doi.org/10.3390/rs14030503

Germann, U., Marco, B., Marco, G., & Maurizio, S. (2015). Peak performance: Radar design for prediction in the Swiss Alps. *Meteorological Technology International*, *4*, 42–45. Retrieved from https://www.meteosuisse.admin.ch/dam/jcr:8f791ccf-6aac-4ea9-a5fc-40bd530db3e7/peak-performance-radar-design-for-prediction.pdf

Giaiotti, D., Nordio, S., & Stel, F. (2003). The climatology of hail in the plain of Friuli Venezia Giulia. *Atmospheric Research*, *67*(68), 247–259. https://doi.org/10.1016/s0169-8095(03)00084-x

Giordani, A., Kunz, M., Bedka, K. M., Punge, H. J., Paccagnella, T., Pavan, V., et al. (2024). Characterizing hail-prone environments using convection-permitting reanalysis and overshooting top detections over south-central Europe. *Natural Hazards and Earth System Sciences*, *24*(7), 2331–2357. https://doi.org/10.5194/nhess-24-2331-2024

Groenemeijer, P., Púčik, T., Holzer, A. M., Antonescu, B., Riemann-Campe, K., Schultz, D. M., et al. (2017). Severe convective storms in Europe: Ten years of research and education at the European Severe Storms Laboratory. *Bulletin of the American Meteorological Society*, *98*(12), 2641–2651. https://doi.org/10.1175/bams-d-16-0067.1

Hand, W. H., & Cappelluti, G. (2011). A global hail climatology using the UK Met Office convection diagnosis procedure (CDP) and model analyses. *Meteorological Applications*, *18*(4), 446–458. https://doi.org/10.1002/met.236

Hentgen, L., Ban, N., Kröner, N., Leutwyler, D., & Schär, C. (2019). Clouds in convection-resolving climate simulations over Europe. *Journal of Geophysical Research: Atmospheres*, *124*(7), 3849–3870. https://doi.org/10.1029/2018jd030150

Hersbach, H., Bell, B., Berrisford, P., Hirahara, S., Horányi, A., Muñoz-Sabater, J., et al. (2020). The ERA5 global reanalysis. *Quarterly Journal of the Royal Meteorological Society*, *146*(730), 1999–2049. https://doi.org/10.1002/qj.3803

Huffman, G., Stocker, E., Bolvin, D., Nelkin, E., & Tan, J. (2023). GPM IMERG final precipitation L3 half hourly 0.1 degree × 0.1 degree V07 [Dataset]. https://doi.org/10.5067/GPM/IMERG/3B-HH/07

Hulton, F., & Schultz, D. M. (2024). Climatology of large hail in Europe: Characteristics of the European severe weather database. *Natural Hazards and Earth System Sciences*, *24*(4), 1079–1098. https://doi.org/10.5194/nhess-24-1079-2024

Huntrieser, H., Schiesser, H. H., Schmid, W., & Waldvogel, A. (1997). Comparison of traditional and newly developed thunderstorm indices for Switzerland. *Weather and Forecasting*, *12*(1), 108–125. https://doi.org/10.1175/1520-0434(1997)012⟨0108:COTAND⟩2.0.CO;2

Huuskonen, A., Saltikoff, E., & Holleman, I. (2014). The operational weather radar network in Europe. *Bulletin of the American Meteorological Society*, *95*(6), 897–907. https://doi.org/10.1175/bams-d-12-00216.1

Isotta, F. A., Frei, C., Weilguni, V., Perčec Tadić, M., Lassègues, P., Rudolf, B., et al. (2014). The climate of daily precipitation in the Alps: Development and analysis of a high-resolution grid dataset from pan-Alpine rain-gauge data. *International Journal of Climatology*, *34*(5), 1657–1675. https://doi.org/10.1002/joc.3794

Jelić, D., Megyeri, O. A., Malečić, B., Belušić Vozila, A., Strelec Mahović, N., & Telišman Prtenjak, M. (2020). Hail climatology along the northeastern Adriatic. *Journal of Geophysical Research: Atmospheres*, *125*(23), e2020JD032749. https://doi.org/10.1029/2020jd032749

Jewell, R., & Brimelow, J. (2009). Evaluation of Alberta hail growth model using severe hail proximity soundings from the United States. *Weather and Forecasting*, *24*(6), 1592–1609. https://doi.org/10.1175/2009WAF2222230.1

Kahraman, A., Kendon, E. J., & Fowler, H. J. (2024). Climatology of severe hail potential in Europe based on a convection-permitting simulation. *Climate Dynamics*, *62*, 6625–6642. https://doi.org/10.1007/s00382-024-07227-w

Kahraman, A., Kendon, E. J., Fowler, H. J., & Wilkinson, J. M. (2022). Contrasting future lightning stories across Europe. *Environmental Research Letters*, *17*(11), 114023. https://doi.org/10.1088/1748-9326/ac9b78

Kendon, E. J., Roberts, N. M., Fowler, H. J., Roberts, M. J., Chan, S. C., & Senior, C. A. (2014). Heavier summer downpours with climate change revealed by weather forecast resolution model. *Nature Climate Change*, *4*(7), 570–576. https://doi.org/10.1038/nclimate2258

Kolendowicz, L., Taszarek, M., & Czernecki, B. (2017). Atmospheric circulation and sounding-derived parameters associated with thunderstorm occurrence in Central Europe. *Atmospheric Research*, *191*, 101–114. https://doi.org/10.1016/j.atmosres.2017.03.009

Kotlarski, S., Keuler, K., Christensen, O. B., Colette, A., Déqué, M., Gobiet, A., et al. (2014). Regional climate modeling on European scales: A joint standard evaluation of the EURO-CORDEX RCM ensemble. *Geoscientific Model Development*, *7*(4), 1297–1333. https://doi.org/10.5194/gmd-7-1297-2014

Kunz, M., & Kugel, P. I. (2015). Detection of hail signatures from single-polarization C-band radar reflectivity. *Atmospheric Research*, *153*, 565–577. https://doi.org/10.1016/j.atmosres.2014.09.010

Labriola, J., Snook, N., Jung, Y., & Xue, M. (2019). Explicit ensemble prediction of hail in 19 may 2013 Oklahoma City thunderstorms and analysis of hail growth processes with several multimoment microphysics schemes. *Monthly Weather Review*, *147*(4), 1193–1213. https://doi.org/10.1175/MWR-D-18-0266.1

Lainer, M. (2024). Hail event on 2022-06-28 in Locarno-Monti (TI), Switzerland: Drone photogrammetry imagery, mask R-CNN model and analysis data of hailstones [Dataset]. *Zenodo*. https://doi.org/10.5281/zenodo.13837508

Lainer, M., Brennan, K. P., Hering, A., Kopp, J., Monhart, S., Wolfensberger, D., & Germann, U. (2024). Drone-based photogrammetry combined with deep learning to estimate hail size distributions and melting of hail on the ground. *Atmospheric Measurement Techniques*, *17*(8), 2539–2557. https://doi.org/10.5194/amt-17-2539-2024

Lapillonne, X., & Fuhrer, O. (2014). Using compiler directives to port large scientific applications to GPUs: An example from atmospheric science. *Parallel Processing Letters*, *24*(1), 1450003. https://doi.org/10.1142/S0129626414500030

Leutwyler, D., Fuhrer, O., Lapillonne, X., Lüthi, D., & Schär, C. (2016). Towards European-scale convection-resolving climate simulations with GPUs: A study with COSMO 4.19. *Geoscientific Model Development*, *9*(9), 3393–3412. https://doi.org/10.5194/gmd-9-3393-2016

Leutwyler, D., Lüthi, D., Ban, N., Fuhrer, O., & Schär, C. (2017). Evaluation of the convection-resolving climate modeling approach on continental scales. *Journal of Geophysical Research: Atmospheres*, *122*(10), 5237–5258. https://doi.org/10.1002/2016JD026013

Löffler-Mang, M., Schön, D., & Landry, M. (2011). Characteristics of a new automatic hail recorder. *Atmospheric Research*, *100*(4), 439–446. https://doi.org/10.1016/j.atmosres.2010.10.026

Lombardo, K., & Bitting, M. (2024). A climatology of convective precipitation over Europe. *Monthly Weather Review*, *152*(7), 1555–1585. https://doi.org/10.1175/MWR-D-23-0156.1

Malečić, B., Cui, R., Demory, M. E., Horvath, K., Jelić, D., Schär, C., et al. (2023). Simulating hail and lightning over the Alpine Adriatic region—A model intercomparison study. *Journal of Geophysical Research: Atmospheres*, *128*(13), e2022JD037989. https://doi.org/10.1029/2022jd037989

Malečić, B., Telišman Prtenjak, M., Horvath, K., Jelić, D., Mikuš Jurković, P., Ćorko, K., & Mahović, N. S. (2022). Performance of HAILCAST and the Lightning Potential Index in simulating hailstorms in Croatia in a mesoscale model – Sensitivity to the PBL and microphysics parameterization schemes. *Atmospheric Research*, *272*, 106143. https://doi.org/10.1016/j.atmosres.2022.106143

Mansell, E. R., Ziegler, C. L., & Bruning, E. C. (2010). Simulated electrification of a small thunderstorm with two-moment bulk microphysics. *Journal of the Atmospheric Sciences*, *67*(1), 171–194. https://doi.org/10.1175/2009jas2965.1

Manzato, A., Cicogna, A., Centore, M., Battistutta, P., & Trevisan, M. (2022). Hailstone characteristics in northeast Italy from 29 years of hailpad data. *Journal of Applied Meteorology and Climatology*, *61*(11), 1779–1795. https://doi.org/10.1175/jamc-d-21-0251.1

Manzato, A., Serafin, S., Miglietta, M. M., Kirshbaum, D., & Schulz, W. (2022). A pan-Alpine climatology of lightning and convective initiation. *Monthly Weather Review*, *150*(9), 2213–2230. https://doi.org/10.1175/MWR-D-21-0149.1

Massacand, A. C., Wernli, H., & Davies, H. C. (1998). Heavy precipitation on the Alpine southside: An upper-level precursor. *Geophysical Research Letters*, *25*(9), 1435–1438. https://doi.org/10.1029/98gl50869

McCaul, E. W., Goodman, S. J., LaCasse, K. M., & Cecil, D. J. (2009). Forecasting lightning threat using cloud-resolving model simulations. *Weather and Forecasting*, *24*(3), 709–729. https://doi.org/10.1175/2008waf2222152.1

Milbrandt, J. A., & Yau, M. K. (2006). A multimoment bulk microphysics parameterization. Part III: Control simulation of a hailstorm. *Journal of the Atmospheric Sciences*, *63*(12), 3114–3136. https://doi.org/10.1175/jas3816.1

Mohr, S., Kunz, M., & Geyer, B. (2015). Hail potential in Europe based on a regional climate model hindcast. *Geophysical Research Letters*, *42*(24), 10904–10912. https://doi.org/10.1002/2015GL067118

Morgan, G., Summers, P., & Kessler, E. (1986). Hailfall and hailstorm characteristics. In *Thunderstorm morphology and dynamics* (2nd ed. ed., p. 237–257). University of Oklahoma Press.

Mroz, K., Battaglia, A., Lang, T. J., Cecil, D. J., Tanelli, S., & Tridon, F. (2017). Hail-detection algorithm for the GPM core observatory satellite sensors. *Journal of Applied Meteorology and Climatology*, *56*(7), 1939–1957. https://doi.org/10.1175/JAMC-D-16-0368.1

Nisi, L., Martius, O., Hering, A., Kunz, M., & Germann, U. (2016). Spatial and temporal distribution of hailstorms in the Alpine region: A long-term, high resolution, radar-based analysis. *Quarterly Journal of the Royal Meteorological Society*, *142*(697), 1590–1604. https://doi.org/10.1002/qj.2771

Noppel, H., Blahak, U., Seifert, A., & Beheng, K. D. (2010). Simulations of a hailstorm and the impact of CCN using an advanced two-moment cloud microphysical scheme. *Atmospheric Research*, *96*(2), 286–301. https://doi.org/10.1016/j.atmosres.2009.09.008

O, S., & Kirstetter, P. (2018). Evaluation of diurnal variation of GPM IMERG-derived summer precipitation over the contiguous US using MRMS data. *Quarterly Journal of the Royal Meteorological Society*, *144*(S1), 270–281. https://doi.org/10.1002/qj.3218

Overeem, A., van den Besselaar, E., van der Schrier, G., Meirink, J. F., van der Plas, E., & Leijnse, H. (2023). EURADCLIM: The European climatological high-resolution gauge-adjusted radar precipitation dataset. *Earth System Science Data*, *15*(3), 1441–1464. https://doi.org/10.5194/essd-15-1441-2023

Panitz, H.-J., Dosio, A., Büchner, M., Lüthi, D., & Keuler, K. (2014). COSMO-CLM (CCLM) climate simulations over CORDEX-Africa domain: Analysis of the ERA-interim driven simulations at 0.44° and 0.22° resolution. *Climate Dynamics*, *42*(11), 3015–3038. https://doi.org/10.1007/s00382-013-1834-5

Petracca, M., Federico, S., Roberto, N., Puca, S., D'Adderio, L. P., Torcasio, R. C., & Dietrich, S. (2024). A 13-year long strokes statistical analysis over the Central Mediterranean area. *Atmospheric Research*, *304*, 107368. https://doi.org/10.1016/j.atmosres.2024.107368

Pham, T. V., Steger, C., Rockel, B., Keuler, K., Kirchner, I., Mertens, M., et al. (2021). Icon in climate limited-area mode (icon release version 2.6.1): A new regional climate model. *Geoscientific Model Development*, *14*(2), 985–1005. https://doi.org/10.5194/gmd-14-985-2021

Piaget, N., Froidevaux, P., Giannakaki, P., Gierth, F., Martius, O., Riemer, M., et al. (2015). Dynamics of a local Alpine flooding event in October 2011: Moisture source and large-scale circulation. *Quarterly Journal of the Royal Meteorological Society*, *141*(690), 1922–1937. https://doi.org/10.1002/qj.2496

Poelman, D. R., Schulz, W., Diendorfer, G., & Bernardi, M. (2016). The European lightning location system EUCLID – Part 2: Observations. *Natural Hazards and Earth System Sciences*, *16*(2), 607–616. https://doi.org/10.5194/nhess-16-607-2016

Poelman, D. R., Schulz, W., & Vergeiner, C. (2013). Performance characteristics of distinct lightning detection networks covering Belgium. *Journal of Atmospheric and Oceanic Technology*, *30*(5), 942–951. https://doi.org/10.1175/JTECH-D-12-00162.1

Portmann, R., Schmid, T., Villiger, L., Bresch, D. N., & Calanca, P. (2024). Modelling crop hail damage footprints with single-polarization radar: The roles of spatial resolution, hail intensity, and cropland density. *Natural Hazards and Earth System Sciences*, *24*(7), 2541–2558. https://doi.org/10.5194/nhess-24-2541-2024

Prein, A. F., & Holland, G. J. (2018). Global estimates of damaging hail hazard. *Weather and Climate Extremes*, *22*, 10–23. https://doi.org/10.1016/j.wace.2018.10.004

Prein, A. F., Langhans, W., Fosser, G., Ferrone, A., Ban, N., Goergen, K., et al. (2015). A review on regional convection-permitting climate modeling: Demonstrations, prospects, and challenges. *Reviews of Geophysics*, *53*(2), 323–361. https://doi.org/10.1002/2014rg000475

Punge, H. J., Bedka, K. M., Kunz, M., & Werner, A. (2014). A new physically based stochastic event catalog for hail in Europe. *Natural Hazards*, *73*(3), 1625–1645. https://doi.org/10.1007/s11069-014-1161-0

Punge, H. J., & Kunz, M. (2016). Hail observations and hailstorm characteristics in Europe: A review. *Atmospheric Research*, *176–177*, 159–184. https://doi.org/10.1016/j.atmosres.2016.02.012

Rädler, A. T., Groenemeijer, P. H., Faust, E., Sausen, R., & Púčik, T. (2019). Frequency of severe thunderstorms across Europe expected to increase in the 21st century due to rising instability. *npj Climate and Atmospheric Science*, *2*(1), 30. https://doi.org/10.1038/s41612-019-0083-7

Reinhardt, T., & Seifert, A. (2006). A three-category ice scheme for LMK (Vol. *6*). Retrieved from http://www.cosmo-model.org/content/model/documentation/newsLetters/newsLetter06/newsLetter_06.pdf

Rösner, B., Benedict, I., van Heerwaarden, C., Weerts, A., Hazeleger, W., Bissolli, P., & Trachte, K. (2019). Sidebar 7.3: The long heat wave and drought in Europe in 2018 [in 'state of the climate in 2018']. *Bulletin of the American Meteorological Society*, *100*(9), S222–S223. https://doi.org/10.1175/2019BAMSStateoftheClimate.1

Rotunno, R., & Houze, R. A. (2007). Lessons on orographic precipitation from the mesoscale Alpine Programme. *Quarterly Journal of the Royal Meteorological Society*, *133*(625), 811–830. https://doi.org/10.1002/qj.67

Saltikoff, E., Haase, G., Delobbe, L., Gaussiat, N., Martet, M., Idziorek, D., et al. (2019). OPERA the radar project. *Atmosphere*, *10*(6), 320. https://doi.org/10.3390/atmos10060320

Sanderson, M. G., Hand, W. H., Groenemeijer, P., Boorman, P. M., Webb, J. D. C., & McColl, L. J. (2015). Projected changes in hailstorms during the 21st century over the UK. *International Journal of Climatology*, *35*(1), 15–24. https://doi.org/10.1002/joc.3958

Schär, C., Ban, N., Fischer, E. M., Rajczak, J., Schmidli, J., Frei, C., et al. (2016). Percentile indices for assessing changes in heavy precipitation events. *Climatic Change*, *137*(1–2), 201–216. https://doi.org/10.1007/s10584-016-1669-2

Schär, C., Fuhrer, O., Arteaga, A., Ban, N., Charpilloz, C., Girolamo, S. D., et al. (2020). Kilometer-scale climate models: Prospects and challenges. *Bulletin of the American Meteorological Society*, *101*(5), E567–E587. https://doi.org/10.1175/BAMS-D-18-0167.1

Schiesser, H. (1990). Hailfall: The relationship between radar measurements and crop damage. *Atmospheric Research*, *25*(6), 559–582. https://doi.org/10.1016/0169-8095(90)90038-E

Schmid, T., Portmann, R., Villiger, L., Schröer, K., & Bresch, D. N. (2024). An open-source radar-based hail damage model for buildings and cars. *Natural Hazards and Earth System Sciences*, *24*(3), 847–872. https://doi.org/10.5194/nhess-24-847-2024

Schulz, W., Cummins, K., Diendorfer, G., & Dorninger, M. (2005). Cloud-to-ground lightning in Austria: A 10-year study using data from a lightning location system. *Journal of Geophysical Research*, *110*(D9), D09101. https://doi.org/10.1029/2004jd005332

Sénési, S., Bougeault, P., Chèze, J., Cosentino, P., & Thepenier, R.-M. (1996). The Vaison-La-Romaine flash flood: Mesoscale analysis and predictability issues. *Weather and Forecasting*, *11*(4), 417–442. https://doi.org/10.1175/1520-0434(1996)011⟨0417:TVLRFF⟩2.0.CO;2

Sideris, I. V., Gabella, M., Erdin, R., & Germann, U. (2014). Real-time radar–rain-gauge merging using spatio-temporal co-kriging with external drift in the Alpine terrain of Switzerland. *Quarterly Journal of the Royal Meteorological Society*, *140*(680), 1097–1111. https://doi.org/10.1002/qj.2188

Soderholm, J. S. (2019). Hailpixel survey data and analysis from 26 November 2018, San Rafael, Argentina [Dataset]. *Zenodo*. https://doi.org/10.5281/zenodo.3383227

Soderholm, J. S., Kumjian, M. R., McCarthy, N., Maldonado, P., & Wang, M. (2020). Quantifying hail size distributions from the sky – Application of drone aerial photogrammetry. *Atmospheric Measurement Techniques*, *13*(2), 747–754. https://doi.org/10.5194/amt-13-747-2020

Sturtevant, J. S. (1995). The severe local storm forecasting primer. *Weather Scratch Meteorol. Serv.*

Taszarek, M., Allen, J., Púčik, T., Groenemeijer, P., Czernecki, B., Kolendowicz, L., et al. (2019). A climatology of thunderstorms across Europe from a synthesis of multiple data sources. *Journal of Climate*, *32*(6), 1813–1837. https://doi.org/10.1175/jcli-d-18-0372.1

Taszarek, M., Allen, J. T., Groenemeijer, P., Edwards, R., Brooks, H. E., Chmielewski, V., & Enno, S.-E. (2020). Severe convective storms across Europe and the United States. Part I: Climatology of lightning, large hail, severe wind, and tornadoes. *Journal of Climate*, *33*(23), 10239–10261. https://doi.org/10.1175/jcli-d-20-0345.1

Taszarek, M., Allen, J. T., Marchio, M., & Brooks, H. E. (2021). Global climatology and trends in convective environments from ERA5 and rawinsonde data. *npj Climate and Atmospheric Science*, *4*(1), 35. https://doi.org/10.1038/s41612-021-00190-x

Thurnherr, I., & Cui, R. (2024). European-wide convection-permitting climate simulation from 2011–2021 using COSMO v6 with HAILCAST and LPI diagnostic: Selected output fields [Dataset]. Retrieved from http://982hdl.handle.net/20.500.11850/701925

Tiedtke, M. (1989). A comprehensive mass flux scheme for cumulus parameterization in large-scale models. *Monthly Weather Review*, *117*(8), 1779–1800. https://doi.org/10.1175/1520-0493(1989)117⟨1779:ACMFSF⟩2.0.CO;2

Toker, E., Ezber, Y., & Sen, O. L. (2021). Numerical simulation and sensitivity study of a severe hailstorm over istanbul. *Atmospheric Research*, *250*, 105373. https://doi.org/10.1016/j.atmosres.2020.105373

Trapp, R. J., Hoogewind, K. A., & Lasher-Trapp, S. (2019). Future changes in hail occurrence in the United States determined through convection-permitting dynamical downscaling. *Journal of Climate*, *32*(17), 5493–5509. https://doi.org/10.1175/JCLI-D-18-0740.1

Trefalt, S., Germann, U., Hering, A., Clementi, L., Boscacci, M., Schröer, K., & Schwierz, C. (2023). *Hail climate Switzerland operational radar hail detection algorithms at MeteoSwiss: Quality assessment and improvement* Technical Report MeteoSwiss No. 284. MeteoSwiss. https://doi.org/10.18751/PMCH/TR/284.HailClimateSwitzerland/1.0

Trefalt, S., Martynov, A., Barras, H., Besic, N., Hering, A. M., Lenggenhager, S., et al. (2018). A severe hail storm in complex topography in Switzerland - Observations and processes. *Atmospheric Research*, *209*, 76–94. https://doi.org/10.1016/j.atmosres.2018.03.007

van Delden, A. (2001). The synoptic setting of thunderstorms in Western Europe. *Atmospheric Research*, *56*(1), 89–110. https://doi.org/10.1016/S0169-8095(00)00092-2

Vergara-Temprado, J., Ban, N., & Schär, C. (2021). Extreme sub-hourly precipitation intensities scale close to the Clausius-Clapeyron rate over Europe. *Geophysical Research Letters*, *48*(3). https://doi.org/10.1029/2020gl089506

Waldvogel, A., Federer, B., & Grimm, P. (1979). Criteria for the detection of hail cells. *Journal of Applied Meteorology and Climatology*, *18*(12), 1521–1525. https://doi.org/10.1175/1520-0450(1979)018⟨1521:CFTDOH⟩2.0.CO;2

Wapler, K. (2013). High-resolution climatology of lightning characteristics within Central Europe. *Meteorology and Atmospheric Physics*, *122*(3–4), 175–184. https://doi.org/10.1007/s00703-013-0285-1

Wells, H. M., Hillier, J., Garry, F. K., Dunstone, N., Clark, M. R., Kahraman, A., & Chen, H. (2024). Climatology and convective mode of severe hail in the United Kingdom. *Atmospheric Research*, *309*, 107569. https://doi.org/10.1016/j.atmosres.2024.107569

Witt, A., Eilts, M. D., Stumpf, G. J., Johnson, J. T., Mitchell, E. D. W., & Thomas, K. W. (1998). An enhanced hail detection algorithm for the WSR-88D. *Weather and Forecasting*, *13*(2), 286–303. https://doi.org/10.1175/1520-0434(1998)013⟨0286:AEHDAF⟩2.0.CO;2

Yair, Y., Lynn, B., Price, C., Kotroni, V., Lagouvardos, K., Morin, E., et al. (2010). Predicting the potential for lightning activity in Mediterranean storms based on the weather research and forecasting (WRF) model dynamic and microphysical fields. *Journal of Geophysical Research*, *115*(D4), D04205. https://doi.org/10.1029/2008jd010868

Yin, L., Ping, F., Xu, H., & Chen, B. (2021). Numerical simulation and the underlying mechanism of a severe hail-producing convective system in east China. *Journal of Geophysical Research: Atmospheres*, *126*(11), e2019JD032285. https://doi.org/10.1029/2019jd032285

Zängl, G., Reinert, D., Rípodas, P., & Baldauf, M. (2015). The ICON (ICOsahedral Non-hydrostatic) modelling framework of DWD and MPI-M: Description of the non-hydrostatic dynamical core. *Quarterly Journal of the Royal Meteorological Society*, *141*(687), 563–579. https://doi.org/10.1002/qj.2378